DOT/FAA/TC-12/16

Federal Aviation Administration
William J. Hughes Technical Center
Aviation Research Division
Atlantic City International Airport
New Jersey 08405

Impact Characteristics of 2024 Aluminum Subject to Penetration by Cylindrical Projectiles

April 2013

Final Report

This document is available to the U.S. public through the National Technical Information Services (NTIS), Springfield, Virginia 22161.

This document is also available from the Federal Aviation Administration William J. Hughes Technical Center at actlibrary.tc.faa.gov.

U.S. Department of Transportation
Federal Aviation Administration

NOTICE

This document is disseminated under the sponsorship of the U.S. Department of Transportation in the interest of information exchange. The U.S. Government assumes no liability for the contents or use thereof. The U.S. Government does not endorse products or manufacturers. Trade or manufacturers' names appear herein solely because they are considered essential to the objective of this report. The findings and conclusions in this report are those of the author(s) and do not necessarily represent the views of the funding agency. This document does not constitute FAA policy. Consult the FAA sponsoring organization listed on the Technical Documentation page as to its use.

This report is available at the Federal Aviation Administration William J. Hughes Technical Center's Full-Text Technical Reports page: actlibrary.tc.faa.gov in Adobe Acrobat portable document format (PDF).

Technical Report Documentation Page

1. Report No. DOT/FAA/TC-12/16	2. Government Accession No.	3. Recipient's Catalog No.
4. Title and Subtitle IMPACT CHARACTERISTICS OF 2024 ALUMINUM SUBJECT TO PENETRATION BY CYLINDRICAL PROJECTILES		5. Report Date April 2013 6. Performing Organization Code
7. Author(s) George Johnson, Bernard Carreon, Giorgio DeVera, Jaya Iyer, Timothy Kostka, and George Mseis		8. Performing Organization Report No.
9. Performing Organization Name and Address University of California, Berkeley Berkeley, CA 94720-1740		10. Work Unit No. (TRAIS) 11. Contract or Grant No.
12. Sponsoring Agency Name and Address U.S. Department of Transportation Federal Aviation Administration William J. Hughes Technical Center Aviation Research Division Aircraft Systems & Structures Branch Atlantic City International Airport, NJ 08405		13. Type of Report and Period Covered Final Report 14. Sponsoring Agency Code ANE-100

15. Supplementary Notes

The Federal Aviation Administration Aviation Research Division COR was Donald Altobelli.

16. Abstract

Aircraft are designed to minimize the risk of catastrophic damage from impact with debris that may result from uncontained engine failure. To accomplish this design, the materials used to fabricate the aircraft must be well understood in terms of their resistance to penetration by projectiles of varying sizes, shapes, and velocities.

The work reported here examines two tempers of a common material used in commercial aircraft: 2024-T3 aluminum sheet and 2024-T351 aluminum plate. Tests were performed involving a range of cylindrical projectiles launched toward the target materials so the axis of the projectile was perpendicular to the target plane. Projectiles were rods made of hardened W1 tool steel or Grade 5 titanium (Ti-6Al-4V) with diameter of 12.7 mm. The projectiles ranged in mass from 9.9 to 50 g and had either a nearly, but not completely, flat impacting face or a hemispherical impacting end. Initial projectile speeds, prior to impact, ranged from 133 to 436 m/s, and the initial energies ranged from 107 to 1234 Joules (J). Target thicknesses ranged from 3.18 to 12.7 mm.

Two sets of tests are reported. In the first set, the goal was to examine the effect of projectile mass, end shape, and effective length on the penetration characteristics of a particular type of target. In these friction and mass tests, all targets were 127-mm-square with a thickness of 6.35 mm. The second set of tests examined three material thicknesses from the same manufacturing lots as those previously tested at National Aeronautics and Space Administration Glenn Research Center and The Ohio State University. Projectiles used for these tests varied by mass and end shape. For each material thickness, the goal was to select a projectile mass that would achieve a ballistic limit of approximately 213 m/s.

Results showed that there was no measureable difference between the penetration characteristics of projectiles of the same mass made of either hardened steel or Grade 5 titanium, and no projectiles showed measureable deformation after impact and penetration. Projectile mass was significant in terms of absorbed energy near the ballistic limit. An increase in projectile mass resulted in an increase in the energy required to initially penetrate the target. The relationship between absorbed energy and projectile mass did not persist once the initial speed was well above the ballistic limit. The effect of friction was significant, with the longer projectiles losing more energy during penetration than the shorter projectiles. The mode of material failure that led to penetration was strongly dependent on the target thickness, the shape of the projectile tip, and the speed at which the projectile impacted the target. In general, hemispherically tipped projectiles caused tearing failures in thinner targets; flat-ended projectiles caused shear plug failure; and fragmentation occurred at high-impact velocities.

17. Key Words Impact, Projectile, 2024 aluminum, Target, Ballistic limit, Plugging, Petaling		18. Distribution Statement This document is available to the U.S. public through the National Technical Information Service (NTIS), Springfield, Virginia 22161. This document is also available from the Federal Aviation Administration William J. Hughes Technical Center at actlibrary.tc.faa.gov.	
19. Security Classif. (of this report) Unclassified	20. Security Classif. (of this page) Unclassified	21. No. of Pages 72	22. Price

Form DOT F 1700.7 (8-72) Reproduction of completed page authorized

ACKNOWLEDGEMENTS

The authors gratefully acknowledge the productive discussions and input from Michael Pereira of the National Aeronautics and Space Administration Glenn Research Center, Tarek Zohdi of the University of California at Berkeley, and especially Donald Altobelli and William Emmerling of the Federal Aviation Administration in the conduct and analysis of this work.

TABLE OF CONTENTS

			Page
EXECUTIVE SUMMARY			xiii
1.	INTRODUCTION		1
	1.1	Background	1
	1.2	Objectives	1
		1.2.1 Friction and Mass Study	1
		1.2.2 The NASA Aluminum Study	2
2.	EXPERIMENTAL SYSTEM AND PROCEDURE		3
	2.1	Pneumatic Projectile Launch System	3
		2.1.1 Helium Gas Gun	4
		2.1.2 Laser Velocity Measurement System	6
		2.1.3 Target Holder and Mount	6
		2.1.4 High-Speed Camera Velocity Measurement System	7
		2.1.5 Catcher Box	9
	2.2	Test Procedure	10
	2.3	Materials	10
		2.3.1 Projectiles	10
		2.3.2 Targets	14
3.	RESULTS		14
	3.1	Friction and Mass Study	14
		3.1.1 Final vs. Initial Projectile Speed	15
		3.1.2 Absorbed Energy	20
		3.1.3 Data Analysis	25
	3.2	The NASA Aluminum Study	28
		3.2.1 Final vs. Initial Projectile Speed	29
		3.2.2 Nature of Damage	31
		3.2.3 Absorbed Energy	36
4.	CONCLUSIONS		39
5.	REFERENCES		40

APPENDICES

A—MACHINE DRAWINGS FOR PROJECTILES USED IN THE FRICTION AND MASS STUDY

B—PRESSURE, SPEED, AND ENERGY DATA

C—STATISTICAL ANALYSIS USING THE R SOFTWARE PACKAGE

LIST OF FIGURES

1	The UCB Pneumatic Gun Setup	3
2	The Pneumatic Gun Setup	4
3	The Pressure Control Valves and Breech End of the Pneumatic Gun	4
4	Projectile Energy vs. Pressure for the Helium Gas Gun	5
5	Laser Velocity Measurement System	6
6	The Target Holder for 127-mm-Square Targets and Target Mount With Target Holder Attached Using Clamps	7
7	Projectile Flight Region Imaged by the High-Speed Camera	8
8	High-Speed Camera Field of Vision for a Typical Test in the Friction and Mass Study	8
9	The Orientation of the High-Speed Camera and the Ring Light Relative to the Projectile Flight Path and a Photograph of the Camera Lens Through the Ring Light	9
10	Catcher Box	9
11	Projectile Design for Flat, Hollow and Flat, Straight Projectiles	12
12	Projectile Design for Standard Flat, Stepped Projectiles	13
13	Design for Projectiles 3a and 7a	13
14	Projectile Design for Hemispherically Tipped Projectiles: Hollow or Straight Stepped	13
15	Final vs. Initial Projectile Speeds for Straight NASA Flat Projectiles Impacting 6.35-mm-Thick Aluminum Plate	15
16	Final vs. Initial Projectile Speeds for Stepped NASA Flat Projectiles Impacting 6.35-mm-Thick Aluminum Plate	15
17	Hole and Plug for a Typical Penetrating NASA Flat Projectile Used in the Friction and Mass Study	16
18	Final vs. Initial Projectile Speeds for 50-g NASA Flat Projectiles Impacting 6.35-mm-Thick Aluminum Plate	17
19	Final vs. Initial Projectile Speeds for 37.5-g NASA Flat Projectiles Impacting 6.35-mm-Thick Aluminum Plate	17

20 Final vs. Initial Projectile Speeds for 25-g NASA Flat Projectiles Impacting 6.35-mm-Thick Aluminum Plate 18

21 Final vs. Initial Projectile Speeds for 12.5-g NASA Flat Projectiles Impacting 6.35-mm-Thick Aluminum Plate 18

22 Final vs. Initial Projectile Speeds for 37.5-g Hemispherically Tipped Projectiles Impacting 6.35-mm-Thick Aluminum Plate 19

23 The Hole and Plug Associated With a Typical Hemispherically Tipped Projectile Impacting 6.35-mm-Thick Aluminum Plate 20

24 Plugs From Penetration of a Hemispherically Tipped and a NASA Flat Projectile With an Unused NASA Flat Projectile Impacting 6.35-mm-Thick Aluminum Plate 20

25 Absorbed vs. Initial Energy for Straight NASA Flat Projectiles Impacting 6.35-mm-Thick Aluminum Plate 21

26 Absorbed vs. Initial Energy for Stepped NASA Flat Projectiles Impacting 6.35-mm-Thick Aluminum Plate 22

27 Absorbed vs. Initial Energy for 50-g NASA Flat Projectiles Impacting 6.35-mm-Thick Aluminum Plate 22

28 Absorbed vs. Initial Energy for 37.5-g NASA Flat Projectiles Impacting 6.35-mm-Thick Aluminum Plate 23

29 Absorbed vs. Initial Energy for 25-g NASA Flat Projectiles Impacting 6.35-mm-Thick Aluminum Plate 23

30 Absorbed vs. Initial Energy for 12.5-g NASA Flat Projectiles Impacting 6.35-mm-Thick Aluminum Plate 24

31 Absorbed vs. Initial Energy for 37.5-g Hemispherically Tipped Projectiles Impacting 6.35-mm-Thick Aluminum Plate 24

32 Initial Projectile Energy at the Ballistic Limit vs. Mass for Stepped Projectiles With NASA Flat Tips Impacting 6.35-mm-Thick Aluminum Plate 28

33 Final vs. Initial Speed for NASA Flat Projectiles Impacting NASA Aluminum Targets 29

34 Final vs. Initial Speed for Hemispherically Tipped Projectiles Impacting NASA Aluminum Targets 29

35 Final vs. Initial Speed for NASA Flat and Hemispherically Tipped Impacting Projectiles 3.18-mm-Thick NASA Aluminum Targets 30

36 Initial vs. Final Speed for NASA Flat and Hemispherically Tipped Impacting Projectiles 6.35-mm-Thick NASA Aluminum Targets 30

37 Photographs of the Exit Side and One Frame of the Postpenetration Video of 3.18-mm-Thick NASA Aluminum Sheet and NASA Flat Projectiles for Test 4 and Test 9 32

38 Photographs of the Exit Side and One Frame of the Postpenetration Video of a Hemispherically Tipped Projectile Penetrating a 3.18-mm-Thick NASA Aluminum Sheet 33

39 Photographs of the Exit Side and One Frame of the Postpenetration Video of 6.35-mm-Thick NASA Aluminum Plate and NASA Flat Projectiles 34

40 Photographs of the Exit Side and One Frame of the Postpenetration Video of a Hemispherically Tipped Projectile Penetrating a 6.35-mm-Thick NASA Aluminum Plate 34

41 Series of Video Frames of Postpenetration Video of Hemispherically Tipped Projectile Penetrating a 6.35-mm-Thick NASA Aluminum Plate 35

42 Video Image Showing the Plug and Fragments for Test Number 9, NASA Flat Projectile Impacting 12.7-mm-Thick NASA Aluminum Plate 36

43 Photograph of the Exit Side and One Frame of the Postpenetration Video of Test Number 5 of the 12.7-mm-Thick NASA Aluminum Plate Penetrated by a NASA Flat Projectile 36

44 Absorbed Energy for NASA Flat Projectiles Impacting NASA Aluminum Targets 37

45 Absorbed Energy for Hemispherically Tipped Projectiles Impacting NASA Aluminum Targets 37

46 Absorbed Energy for NASA Flat and Hemispherically Tipped Projectiles Impacting 3.18-mm-Thick NASA Aluminum Targets 38

47 Absorbed Energy for NASA Flat and Hemispherically Tipped Projectiles Impacting 6.35-mm-Thick NASA Aluminum Targets 38

48 Absorbed Energy for NASA Flat and Hemispherically Tipped Projectiles Impacting 12.7-mm-Thick NASA Aluminum Targets 39

LIST OF TABLES

1	Design Parameters for the Projectiles Used in the Friction and Mass Tests	12
2	Design Parameters for the Projectiles Used in the NASA Aluminum Study	12
3	Coefficients of Fit of Equation 2 to Data From 37.5-g Straight NASA Flat Projectiles Comparing Projectile 3 (Steel) to Projectile 3a (Titanium)	26
4	Statistics for all Straight and Stepped Projectiles With the NASA Flat Tip	26
5	Coefficients of Fit of Equation 3 to Data From All NASA Flat Projectiles Comparing Stepped Projectiles to Straight Projectiles	27
6	Statistics for All Straight and Stepped Projectiles With Hemispherical Tip	27

LIST OF ACRONYMS

FAA	Federal Aviation Administration
J	Joules
NASA	National Aeronautics and Space Administration
NASA-GRC	National Aeronautics and Space Administration-Glenn Research Center
OSU	The Ohio State University
UCB	University of California, Berkeley

EXECUTIVE SUMMARY

Aircraft are designed to minimize the risk of catastrophic damage from impact from debris resulting from uncontained engine failure. To accomplish this design, the materials used to fabricate the aircraft must be well understood in terms of their resistance to penetration by projectiles of varying sizes, shapes, and velocities.

This report examines target materials from two tempers of a common material used in commercial aircraft: 2024-T3 aluminum sheet and 2024-T351 aluminum plate. Tests were performed involving a range of cylindrical projectiles launched toward the target material so the axis of the projectile was perpendicular to the plane of the target. Projectiles were rods made of hardened W1 tool steel or Grade 5 titanium (Ti-6Al-4V) with a diameter of 12.7 mm. The projectiles ranged in mass from 9.9 to 50 g and had either a nearly, but not completely, flat impacting face or a hemispherical impacting end. Initial projectile speeds, prior to impact, ranged from 133 to 436 m/s, and the initial energies ranged from 107 to 1234 Joules (J). Target thicknesses ranged from 3.18 to 12.7 mm.

Two sets of tests are reported. In the first test set, the goal was to examine the effect of projectile mass, end shape, and effective length on the penetration characteristics of a particular type of target. In these friction and mass tests, all targets were 127-mm-square plates of 6.35-mm-thick material. The second test set examined three material thicknesses from the same lots as those previously tested at National Aeronautics and Space Administration Glenn Research Center. Projectiles used for these tests varied by mass and end shape, but for each material thickness, the goal was to select a projectile mass that would achieve a ballistic limit of approximately 213 m/s (or approximately 700 ft/s).

Results showed that there was no measureable difference between the penetration characteristics of projectiles of the same mass made of either hardened steel or Grade 5 titanium. Projectile mass was significant in terms of absorbed energy near the ballistic limit. An increase in projectile mass resulted in an increase in the energy required to initially penetrate the target. The relationship between absorbed energy and projectile mass did not persist once the initial speed was well above the ballistic limit. The effect of friction was significant, with longer projectiles losing more energy during penetration than shorter projectiles. The mode of material failure that led to penetration was strongly dependent on the thickness of the target, the shape of the projectile tip, and the speed at which the projectile impacted the target. In general, hemispherically tipped projectiles caused tearing failures in thinner targets; flat-ended projectiles caused shear plug failure; and fragmentation occurred at high-impact velocities for the thicker targets.

1. INTRODUCTION.

1.1 BACKGROUND.

Over the past several years, the University of California, Berkeley (UCB), sponsored by the Federal Aviation Administration (FAA) Aircraft Catastrophic Failure Prevention Program, has participated with the FAA, The Boeing Company, National Aeronautics and Space Administration (NASA), Lawrence Livermore National Laboratory, and SRI International in research directed at enhancing the safety of commercial aircraft in the case of uncontained engine failure. The program focused on characterizing the response of various aircraft materials to ballistic impact. This study focused on the response of 2024-T3 aluminum sheet and 2024-T351 aluminum plate.

1.2 OBJECTIVES.

There are two test sets included in this report. The first test set, the friction and mass study, examined the amount of energy lost due to friction between the projectile and the hole through which the projectile passes. This first test set also examined the effect of projectile mass on the ballistic characteristics of this material. The second test set, the NASA aluminum study, provided independent measurements of a material and projectile combination that were previously tested at NASA. This test set also investigated the difference in energy lost during penetration between a flat-tipped cylindrical projectile and a hemispherically tipped projectile of the same mass.

1.2.1 Friction and Mass Study.

Previous work at UCB [1] suggested that friction between a penetrating projectile and the target through which it passes may play a significant role in how much energy is removed from the projectile during the penetration process.

The purpose of this set of tests was to examine two main effects in the penetration of projectiles through 6.35-mm-thick flat plates of 2024-T351 aluminum. The objectives were to (1) quantify the amount of energy that is lost due to the frictional interaction between the sides of a projectile and sides of the hole in a plate through which the projectile is passing and (2) determine the effect of projectile mass on energy loss during plate penetration. To accomplish these goals, a set of ten projectile types were designed and tested. Eight projectile types within this set consisted of four masses (nominally 50, 37.5, 25, and 12.5 g) and for each mass, two outside diameter configurations (straight and stepped). All projectiles within this set of projectile types had the same nominal diameter at the impacting tip (12.7 mm) and all had the same tip shape (the “NASA Flat” tip, described in more detail in section 2.3.1). Straight projectiles had a uniform 12.7-mm diameter along a 50.8-mm distance behind the impact tip, while stepped projectiles presented a cylindrical region of the nominal 12.7-mm diameter for only 6.35 mm behind the impact tip. Thus, to fully penetrate the target, the lateral surface of a straight projectile was in contact with the hole through which it was passing for the full length of the projectile (50.8 mm). For the stepped projectiles, the interaction length between the surface of the projectile and the hole was only 6.35 mm. The expectation was that this decreased

interaction length would result in less kinetic energy loss for the stepped projectiles compared to the straight projectiles.

In addition, two other projectile shapes were examined in this study. These projectiles had a hemispherical impact tip, rather than the NASA Flat tip. Both had a nominal mass of 37.5 g, but differed in their side profile (straight versus stepped).

The friction and mass study used targets cut from a single 6.35-mm-thick plate of 2024-T351 aluminum. Projectiles varied in axial cross section and mass, with about ten shots taken for each projectile type. The projectile shapes (cross sections) consisted of two distinct types: those that were continuous right circular cylinders of 12.7-mm diameter along the full length of the projectile, and those that had a reduced-diameter "tail" section following a relatively short 12.7-mm-diameter section that would create the hole in the target plate. These two shapes were intended to provide extreme cases for each projectile mass and impact face, one that presented maximum frictional loss and one that presented minimal frictional loss.

1.2.2 The NASA Aluminum Study.

The second test set, NASA aluminum study, provided independent measurements of the same manufacturing lots of 2024 aluminum material that was previously tested at the National Aeronautics and Space Administration-Glenn Research Center (NASA-GRC) and The Ohio State University (OSU) under a separate FAA Grant. NASA supplied the 2024 aluminum targets for the second test set. In addition, a comparison of ballistic limits was made between hemispherically and flat-tipped, cylindrical projectiles at the same weight. All projectiles were machined from 12.7-mm-diameter hardened steel or titanium rods and had impacting faces that were either (1) nearly, but not completely, flat (referred to as "NASA Flat" in this report) with a very large tip radius of 69.85 mm to prevent edge contact or (2) hemispherical. In all cases, penetration of a projectile required the ballistic formation of a hole in the target plate that was nearly the same size as the projectile's largest diameter (12.7 mm). Projectile mass was chosen so the expected ballistic limit for each plate thickness would be approximately 213 m/s (approximately 700 ft/s), corresponding to high-velocity turbine engine fragment release speeds.

Target thicknesses of 3.18, 6.35, and 12.7 mm were used. The 3.18-mm sheet material was 2024-T3, and the thicker plate material was 2024-T351. The projectile masses selected for the three target thicknesses were 9.9 g for the 3.18-mm sheet, 13 g for the 6.35-mm plate, and 25 g for the 12.7-mm plate. Tests were performed using both NASA Flat projectiles and projectiles with hemispherical ends for the 3.18- and 6.35-mm-thick material. Only NASA Flat projectiles were used for the 12.7-mm plate test.

Results for the tests on the NASA-provided aluminum targets show that the ballistic limit for both NASA Flat and hemispherically tipped projectiles was close to the ballistic limit of 213 m/s only for the 3.18-mm sheet. For the other two thicknesses, the measured ballistic limit was greater for the hemispherically tipped projectiles than for the NASA Flat projectiles. The difference between the two tip shapes was associated with differences in the way the target material near the impact deformed and eventually failed. For the 3.18-mm sheet, NASA Flat projectiles produced shear plugs and a hole that were only slightly smaller than the diameter of the projectile; hemispherically tipped projectiles produced smaller plugs than those produced by

the NASA Flat projectiles, and the target sheet tore in a number of locations around the hole to accommodate the projectile as it passed through. The results for the NASA Flat projectiles penetrating the 6.35-mm plate were similar to those for the lightest projectiles used in the friction and mass study. The hemispherically tipped projectiles, on the other hand, exhibited considerably different behavior. Full projectile penetration did not occur until the projectile energy was sufficient to produce fragments near the edge of the hole, a mode of deformation not observed in the friction and mass study. The results for the 12.7-mm plate showed considerable variation among projectiles with similar initial energy.

2. EXPERIMENTAL SYSTEM AND PROCEDURE.

2.1 PNEUMATIC PROJECTILE LAUNCH SYSTEM.

All test shots were performed using a pneumatic gun setup consisting of a helium gas gun, a laser velocity measurement system, a target holder and mount, one or two high-speed cameras used for velocity measurement, and a catcher box. A photograph of the setup is shown in figure 1, while a schematic is shown in figure 2.

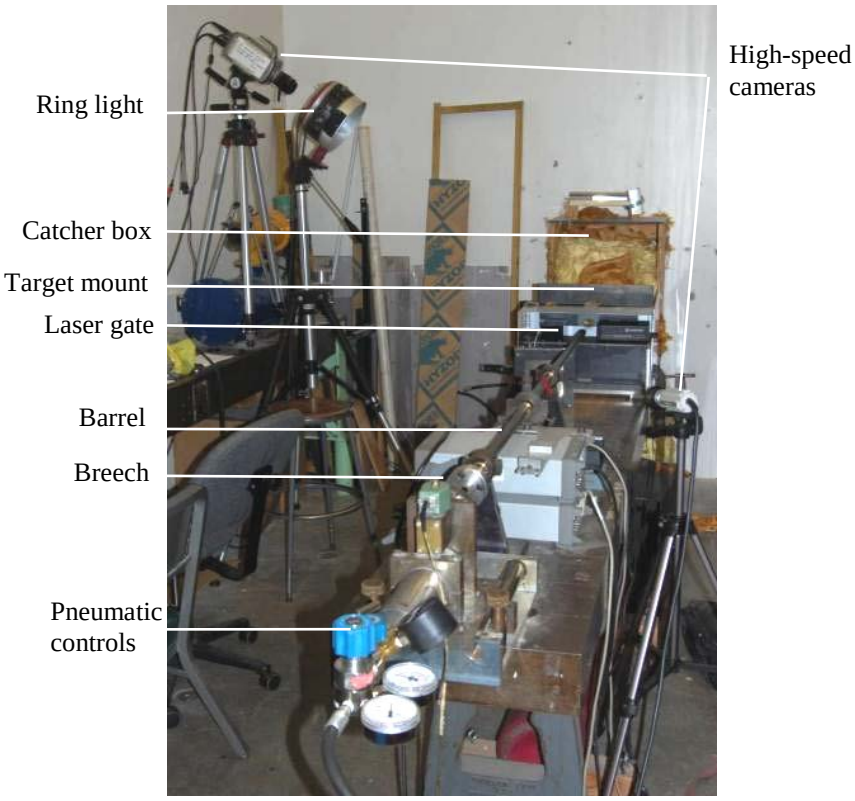

Figure 1. The UCB Pneumatic Gun Setup

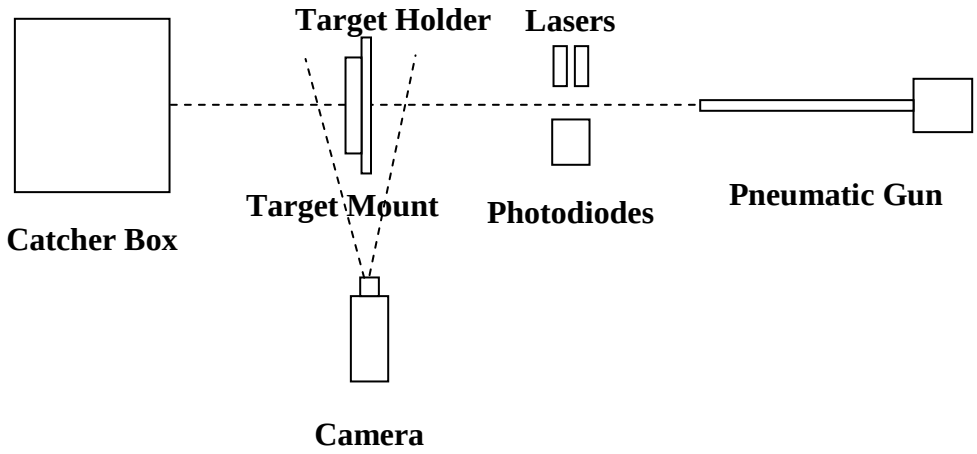

Figure 2. The Pneumatic Gun Setup

2.1.1 Helium Gas Gun.

All test shots were performed with a high-pressure pneumatic gun that used compressed industrial helium. A regulator valve allowed for pressure up to approximately 11 MPa. The gun barrel was approximately 1.87 m long with a 12.73-mm diameter. An exterior trigger controlled a solenoid valve between a breech pressure chamber and the gun barrel, allowing for firing of the gun when the pressure was released. A photograph of the breech end of the pneumatic gun is shown in figure 3.

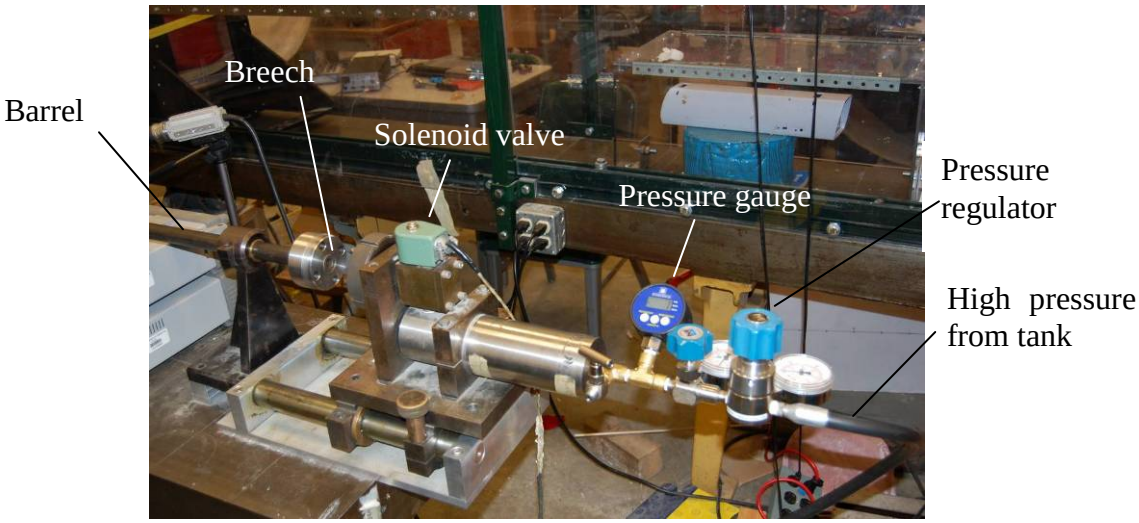

Figure 3. The Pressure Control Valves and Breech End of the Pneumatic Gun

Projectile speed was reasonably predicted by a nearly linear relationship between initial projectile energy and pressure. Figure 4 shows results of speed versus pressure of shots taken for the studies reported here (the friction and mass study and the NASA aluminum study) over a period of approximately 24 months. Projectiles ranged in mass from approximately 9.85 to 50 g, and, sometimes, a nylon sabot (with mass of 2.3 g) was used to maintain projectile alignment in

the gun barrel. The trends shown in figure 4 were used to estimate the pressure necessary to achieve a particular projectile speed, but the actual speed was determined using either the laser gate or the high-speed camera measurements.

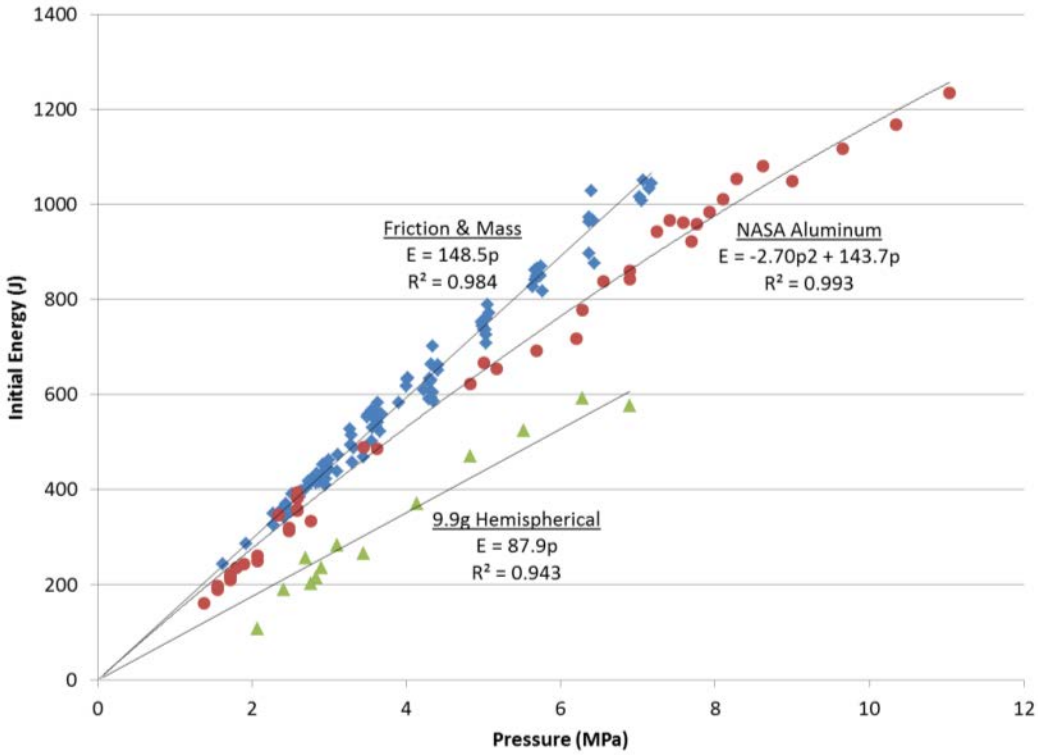

Figure 4. Projectile Energy vs. Pressure for the Helium Gas Gun

Three data sets are shown in figure 4. All the shots for the friction and mass study are shown in one set (blue diamonds), with the straight-line fit providing a good estimate to the data throughout the range of pressures. The shots for the NASA aluminum study (red circles) did not converge to a single fit. Instead, it was observed that the shortest, lightest projectiles (9.9-g mass with hemispherical tips) (green triangles) achieved lower speeds, and thus lower energies, than what was expected from the rest of the shots in this study. As a result, these shots are shown separately, with a separate, straight-line fit. The slope of this line is considerably different than the slope of the line for the friction and mass study or the initial slope of the remaining shots for the NASA aluminum study. A quadratic fit was used for the majority of the NASA aluminum shots as the high-pressure data shows a clear trend away from a linear fit. In some cases, the projectile speeds at these higher pressures exceeded the sound speed in the ambient room air. The data suggest a possible dependence on projectile length, but this was not examined in detail.

Note that if the gas pressure were constant as the projectile moved down the barrel, the work done per unit pressure on the projectile due to this force would be approximately 230 J/MPa. This upper bound for the projectile energy is only about 60% larger than that found in the straight-line fit to the friction and mass data in figure 4.

2.1.2 Laser Velocity Measurement System.

The laser velocity measurement system, which was used to acquire the initial projectile velocity for some of the reported measurements, consisted of two helium-neon lasers and two photodiode light detectors. The lasers were 6.35 cm apart and focused at the light detectors. When the projectile passed through each laser beam, a universal counter or timer would detect a voltage drop in the corresponding photodiode circuit. Projectile velocity was calculated using the time between voltage drops. The laser velocity measurement system is shown in figure 5.

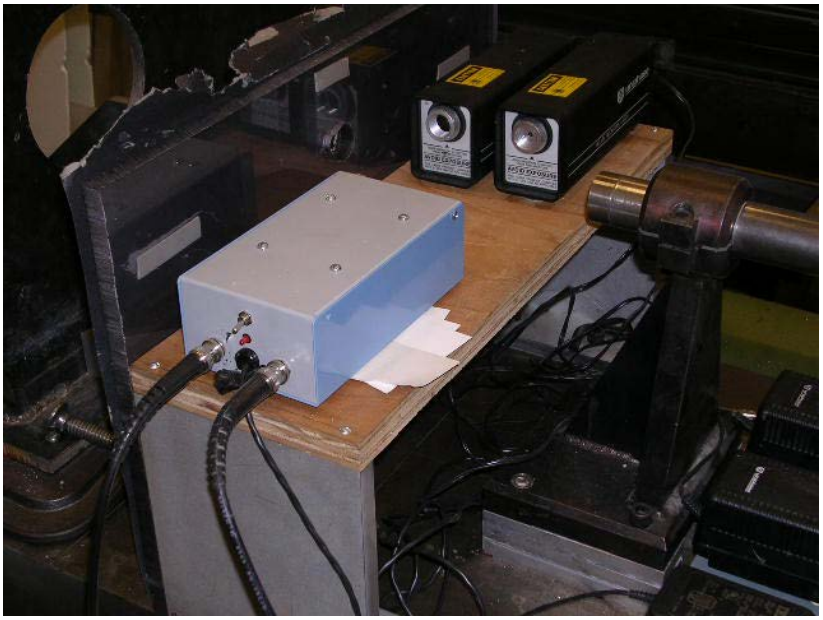

Figure 5. Laser Velocity Measurement System

2.1.3 Target Holder and Mount.

All targets were secured between two 12.7-mm-thick steel plates. For the tests using larger (30.5-cm-square) targets, both plates were 35.6 by 35.6 cm with 25.4- by 25.4-cm openings cut out of the center. Steel bolts at each corner of the holder were used to hold the plates together and secure the target between them. For tests using smaller (15.2-cm-square) targets, the holder plates were 20.3 by 20.3 cm with 12.7- by 12.7-cm openings cut from the center.

The target holder was mounted onto a steel angle bracket with a 15.2-cm-diameter hole to allow the projectile to pass through. This angle bracket is referred to as the “target mount.” The target holder was secured to the target mount using clamps at each corner. The target mount was attached to the steel table using four screws. The target mount and target holder is shown in figure 6.

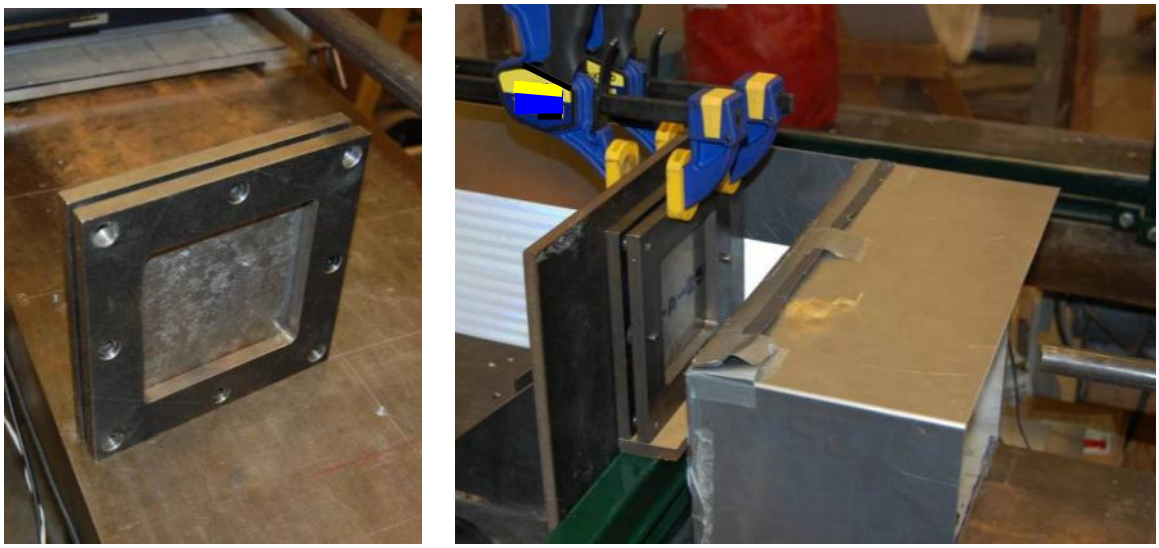

(a) (b)

Figure 6. The (a) Target Holder for 127-mm-Square Targets and (b) Target Mount With Target Holder Attached Using Clamps

2.1.4 High-Speed Camera Velocity Measurement System.

Projectile velocity, as well as the velocity of the plug that was ejected during the penetration of the target, was measured using a Phantom V5.1 high-speed camera [2] with a Nikkor 35—70-mm lens. With the camera situated on a tripod approximately 1.5 m perpendicular to and 0.3 m above the path of the projectile, a field of view 0.15 m ahead of and 0.45 m behind the target was possible. A high-intensity ring light was used to illuminate the field of vision. Earlier tests performed in this study involving the NASA aluminum targets used a white background with a matte finish. For these tests, the exposure time was typically 10 μs. In later tests performed in this study, retro-reflective tape was used behind the path of the projectile to minimize the amount of lighting necessary to achieve a sharp image at the minimum possible exposure time (2 μs). Figure 7 shows a high-speed photograph of the region, with no target mounted. Figure 8 shows an image from the high-speed camera during one test. Both the plug and projectile after penetration are visible in this image. The projectile is moving from right to left, and is preceded by the plug that was ejected during the penetration event. For reference, the projectile is 50.8 mm long.

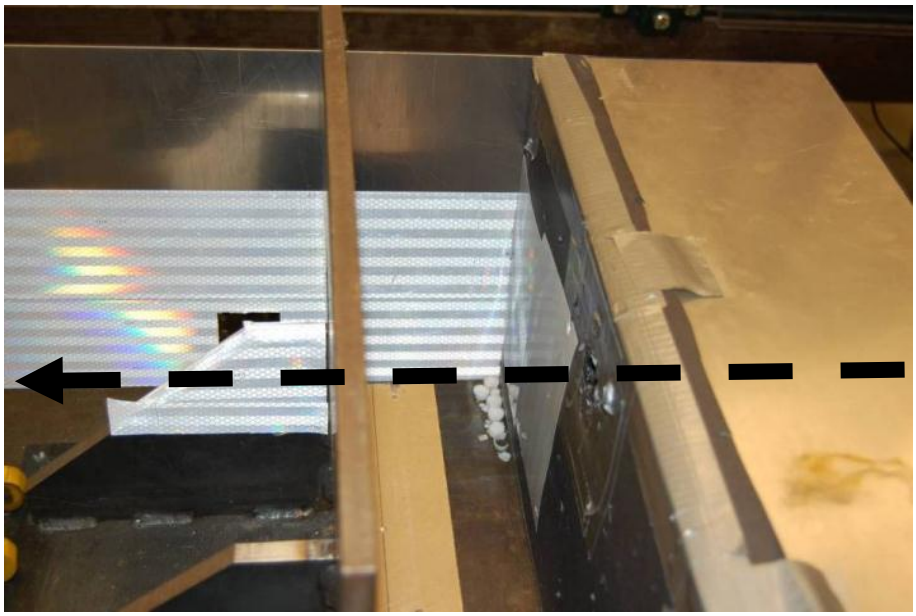

Figure 7. Projectile Flight Region Imaged by the High-Speed Camera

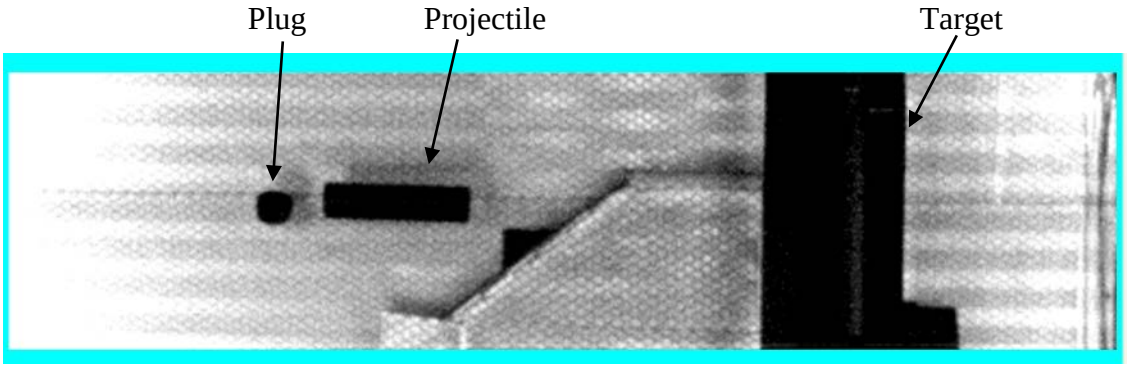

Figure 8. High-Speed Camera Field of Vision for a Typical Test in the Friction and Mass Study

Projectile shots were recorded at frame rates between 4,000 and 16,000 frames per second. Recordings were analyzed using Phantom Camera Control Software [2]. The high-speed camera setup is shown in figure 9.

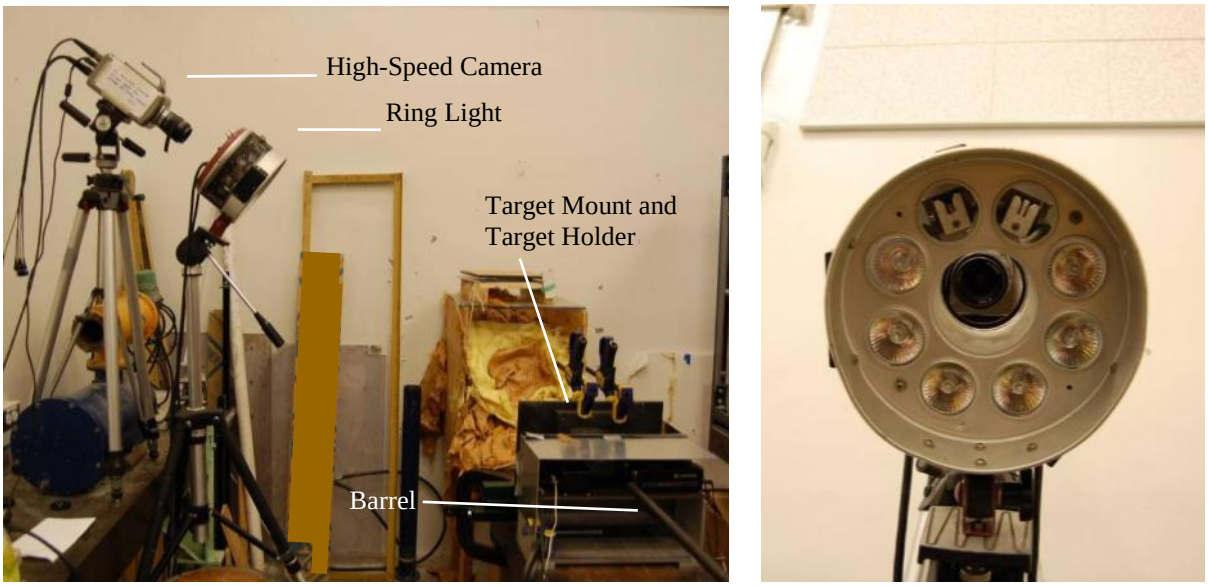

(a) (b)

Figure 9. The (a) Orientation of the High-Speed Camera and the Ring Light Relative to the Projectile Flight Path and (b) a Photograph of the Camera Lens Through the Ring Light

2.1.5 Catcher Box.

The catcher box, shown in figure 10, consisted of a wooden box filled with Zylon® sheets and backed by a 12.7-mm-thick steel plate. After passing through the target, the catcher box was intended to stop the projectiles to prevent a ricochet effect from the projectile or the plug.

Figure 10. Catcher Box

2.2 TEST PROCEDURE.

A summary of the test procedure is given below.

1. The target was placed in the target holder and centered in the holder plates.

2. The target holder was placed on the front of the target mount using clamps. A shim was used below the target holder to adjust the holder height ensuring that the projectile would hit the center of the target.

3. The projectile was loaded into the breech of the gun.

4. The universal counter was set to properly determine the time required for the projectile to pass both laser beams.

5. The pressure in the breech chamber was set using the helium tank's regulator valve. After the desired pressure was reached, the regulator valve was closed.

6. The high-speed camera was set to record, waiting for the exterior trigger. The high-intensity lamps were turned on.

7. The exterior trigger was pressed.

8. The recorded shot was analyzed using the Phantom software.

The penetration angles were determined for some tests using a digital "feeler gage" on a computer numerically controlled machine. The gage was first used to determine the center (x and y coordinates) of the hole at the plate's front (impact) surface. Then, the center of the hole was determined at the midplane of the plate (at a depth of 6.35 cm). A line was formed through the centers of the two holes. The penetration angle is the angle between the line made from the centers and the line normal to the plate.

2.3 MATERIALS.

2.3.1 Projectiles.

All projectiles were machined from 12.7-mm (0.5-in.)-diameter rod of either W1 tool steel or titanium 6Al–4V (Grade 5 Ti-6-4). After machining, steel projectiles were heat-treated to achieve a nominal Rockwell C60 surface hardness. The heat treatment was consistent with case hardening for W1 tool steel, but the diameter of the rod may have resulted in through-hardened material. The actual hardening depth was not examined. The material used depended on the desired projectile mass; steel was used for projectiles with mass of 28 g and above, and titanium was used for projectiles with mass of 37.5 g and below. There was some overlap in the intermediate mass range, which helped to determine whether there was any difference in the behavior of projectiles made from these two materials.

Two tip shapes were used: the NASA Flat tip and a hemispherical tip. The NASA Flat tip has a slightly rounded impacting face (69.85-mm radius) and a finite radius at the transition between

the impacting face and the shank of the projectile that avoids a sharp corner in this region. The 69.85-mm radius was chosen to allow the projectile to experience up to a 5° rotation upon impact and still have the projectile hit the target on some part of its face without hitting the target with a sharp corner. Beyond this maximum angle of incidence of 5°, the first point of impact was along the transition region, which has a 0.79-mm radius. The hemispherically tipped projectiles had a radius of 6.35 mm at one end, allowing a smooth transition from the tip shank of the projectile.

Projectiles are classified as either straight or stepped based on whether the diameter is a constant 12.7 mm for the entire length of the projectile after the tip transition to the rear end (straight) or the diameter is reduced after a relatively short 6.35-mm length at the nominal 12.7-mm diameter (stepped). Stepped projectiles were designed to elucidate the effect of the frictional interaction between the sides of the projectile and the hole that is created as the projectile passes through the target. To ensure that the projectiles traveled through the barrel without rotation, a small nylon sabot was used at the tail end of the stepped projectiles.

To achieve the desired mass for some of the lightest projectiles, material was removed by drilling a prescribed depth into the rear end of the projectile. In all but one case, such hollowed projectiles used a single, standard machine tool, leaving a uniform wall thickness toward the tail end of the projectile.

Thus, projectiles are characterized by five parameters: mass, tip shape, material, straight or stepped, and hollowed or not. The terms stepped and hollowed are mutually exclusive because only straight projectiles have hollow sections at their tail end, if necessary, to reduce the mass.

The detailed design parameters for the ten projectiles used in the first test set, the friction and mass tests, are shown in table 1. The design parameters for the projectiles used in the second test set, the NASA aluminum study, are shown in table 2. It should be noted that projectiles in the tables marked as flat have the NASA Flat tip. The design drawings for each projectile are shown in figures 11 through 14. (Note: All linear dimensions in these figures are in millimeters.) Additional specimen manufacture drawings are provided in appendix A, and for machining purposes, the specifications of the projectiles are given in inches.

Table 1. Design Parameters for the Projectiles Used in the Friction and Mass Tests

Projectile Designator (Tip-Mass-Material-Geometry)	Design Number	Design Drawing (Figure No.)	Target Thickness (mm)	Total Length L (mm)	Hole or Extension Diameter A (mm)	Hole or Extension Length B (mm)
Flat-50 g-Steel-Straight	1	11	6.35	50.80	--	--
Flat-50 g-Steel-Stepped	2	12	6.35	75.03	10.16	68.68
Flat-37.5 g-Steel-Hollow	3	11	6.35	50.80	7.37	37.72
Flat-37.5 g-Ti-Straight*	3a	13(a)	6.35	75.77	10.16	24.97
Flat-37.5 g-Steel-Stepped	4	12	6.35	55.37	10.16	49.02
Flat-25 g-Ti-Hollow	5	11	6.35	50.80	6.35	23.88
Flat-25 g-Ti-Stepped	6	12	6.35	66.04	10.16	59.69
Flat-12.5 g-Ti-Hollow**	7a	13(b)	6.35	50.80	See figure 13(b)	
Flat-12.5 g-Ti-Stepped	8	12	6.35	31.72	10.16	25.37
Hemi-37.5 g-Steel-Hollow	9	14(a)	6.35	57.15	8.20	40.64
Hemi-37.5 g-Steel-Stepped	10	14(b)	6.35	53.59	10.16	53.59

*This projectile is straight for 50.80 mm along the length, then has a tail extension to achieve the desired mass of 37.5 g. See figure 13(a).
**This projectile has a two-step hollowed region, as shown in figure 13(b).

Table 2. Design Parameters for the Projectiles Used in the NASA Aluminum Study

Projectile Designator (Tip-Mass-Material-Geometry)	Design Drawing (Figure No.)	Target Thickness (mm)	Total Length L (mm)	Hole Diameter A (mm)	Hole Depth B (mm)
Flat-28 g-Steel-Straight	11	12.70	28.58	--	--
Flat-13 g-Ti-Straight	11	6.35	22.86	--	--
Flat-9.9 g-Ti-Hollow	11	3.18	22.86	9.53	10.11
Hemi-13 g-Ti-Straight	14(a)	6.35	24.82	--	--
Hemi-9.9 g-Ti-Hollow	14(a)	3.18	24.82	9.53	10.11

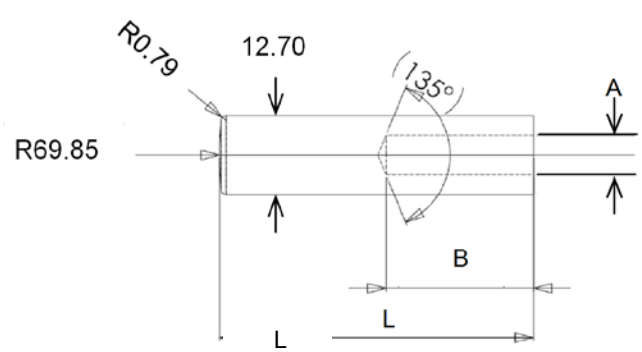

Figure 11. Projectile Design for Flat, Hollow and Flat, Straight Projectiles

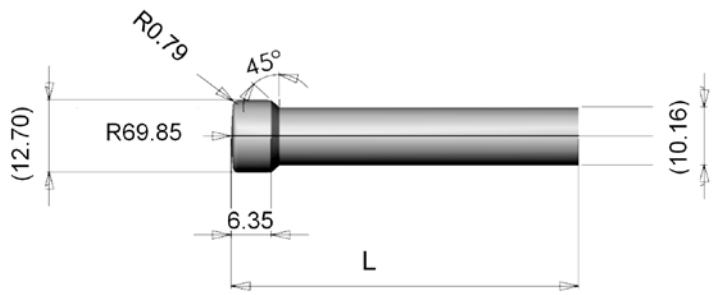

Figure 12. Projectile Design for Standard Flat, Stepped Projectiles

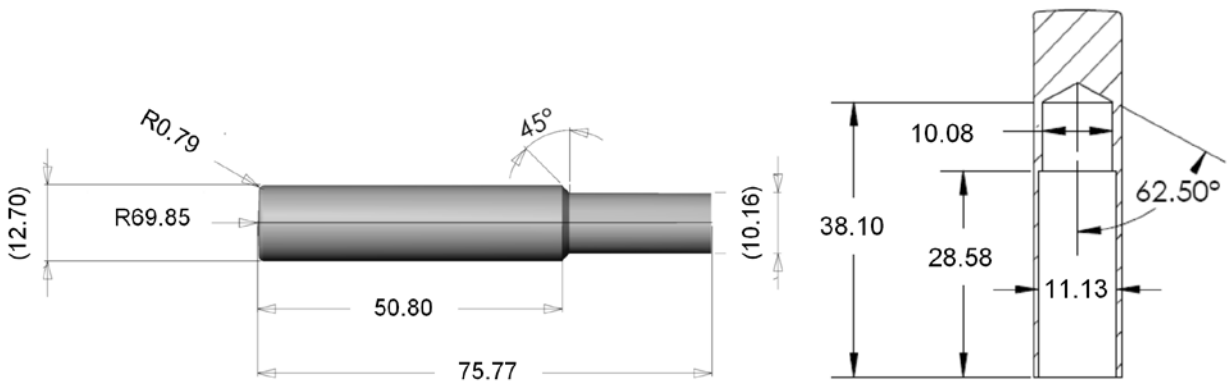

(a) (b)

Figure 13. Design for Projectiles (a) 3a and (b) 7a

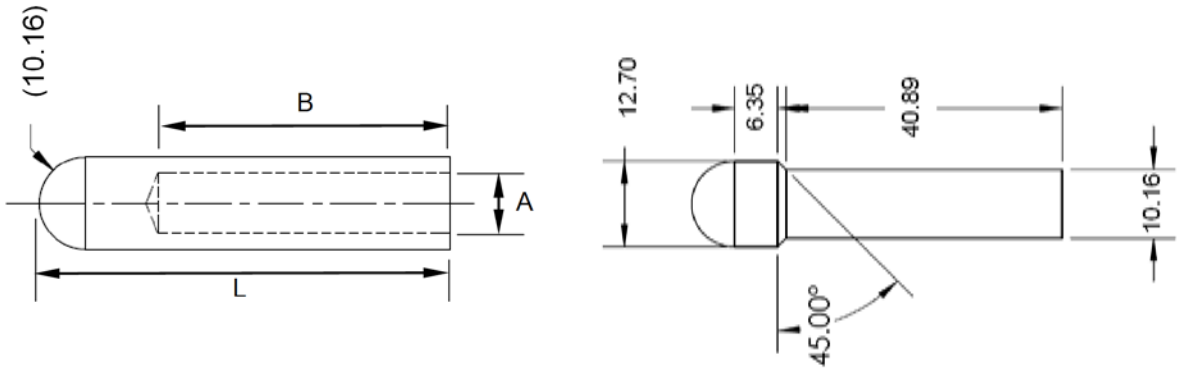

(a) (b)

Figure 14. Projectile Design for Hemispherically Tipped Projectiles: (a) Hollow or Straight (b) Stepped

2.3.2 Targets.

Aluminum 2024-T351 was used as the target material for all tests except for the 3.18-mm targets, which were aluminum 2024-T3 material. For the friction and mass study, all targets were cut into 152-mm squares from a single 6.35-mm-thick aluminum 2024-T351 plate.

The material for the NASA aluminum study was three different thicknesses: 3.2, 6.35, and 12.7 mm. Square plates (30.4 by 30.4 cm) of the 3.2 and the 6.35 mm thicknesses were tested as received from NASA-GRC.

3. RESULTS.

3.1 FRICTION AND MASS STUDY.

As noted in the introduction, the purpose of this set of tests was to examine the effects of (1) the frictional interaction between a penetrating projectile and the target through which it passes, and (2) the mass of the projectile on the energy absorbed. The tests reported below use straight and stepped projectiles with the same mass and tip shape (NASA Flat or hemispherical) to quantify the effect of friction. Projectiles of four different masses for each projectile profile and tip shape were used to examine the effect of mass.

The initial and final velocities of all ten types of projectiles (straight and stepped, NASA Flat and hemispherically tipped, and several masses) were examined. In all cases, at least one projectile was launched at a speed below that required for full penetration (i.e., below the ballistic limit) to identify the ballistic limit speed. For these tests, all NASA Flat projectiles produced a relatively clean shear plug, which had a diameter slightly less than the diameter of the projectile. Little, if any, tearing of the material occurred as the projectile passed through the plate. The hemispherically tipped projectiles produced somewhat smaller plugs that were more heavily deformed to conform with the shape of the impacting surface. The hole at the exit side of the plate generally showed “petaling” where the material exhibited tensile fracture to accommodate the passing projectile.

Section 3.1.1 examines the final versus initial kinetic energies for each of the cases considered. The kinetic energy of both the plug and the projectile were used to determine the final kinetic energy. In the case of the lightest projectiles, the energy of the plug made a substantial contribution to the total final kinetic energy.

Section 3.1.2 provides a statistical analysis of the data with the goal of quantifying the effects of friction, mass, and material on the ballistic characteristics of the various projectiles. It was determined that the friction, as observed in the energy difference between the projectiles with straight sides and stepped sides, had a statistically significant effect on the absorbed energy. There was no apparent difference in the ballistic characteristics of similarly sized and shaped projectiles made of hardened steel or titanium. Projectile mass was shown to play a significant role in determining the energy absorbed near the ballistic limit, but its role at higher speeds was not clear.

3.1.1 Final vs. Initial Projectile Speed.

Figures 15 and 16 show the final projectile speed versus the initial projectile speed for the straight and the stepped NASA Flat projectiles, respectively. As noted in section 2.3.2, all targets for the friction and mass study had a thickness of 6.35 mm. Final speeds reported as negative numbers indicate that the projectile rebounded toward the barrel from the target plate. Detailed results for each test shot performed are provided in appendix B.

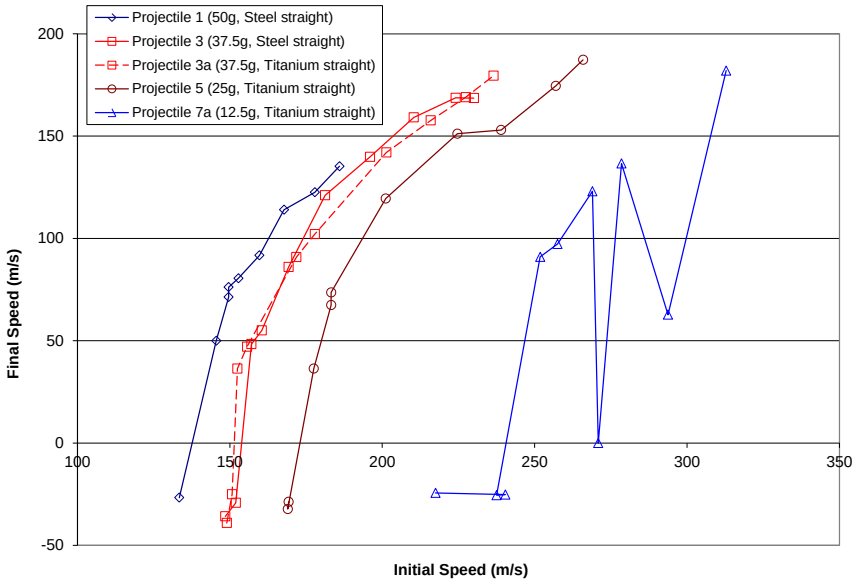

Figure 15. Final vs. Initial Projectile Speeds for Straight NASA Flat Projectiles Impacting 6.35-mm-Thick Aluminum Plate

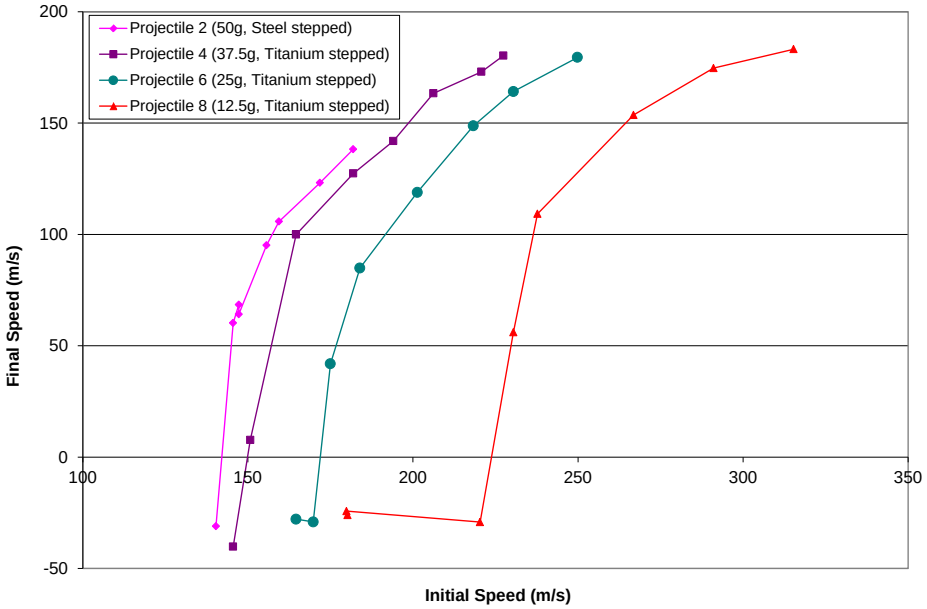

Figure 16. Final vs. Initial Projectile Speeds for Stepped NASA Flat Projectiles Impacting 6.35-mm-Thick Aluminum Plate

The nature of the damage to the plate was the same for all penetrating projectiles: a shear plug was ejected prior to the projectile passing through the plate. The edges of the plug were not completely smooth, and the plug was not a perfect right circular cylinder. Rather, the diameter of the plug was somewhat larger at the impacting face than at the exit face. The slightly rounded shape of the NASA Flat impact face was impressed upon the plug in the region of impact, and the plug diameter at that location was, in general, almost equal to the projectile diameter. The hole in the plate was polished by the projectile as it passed through, leaving the surface considerably smoother than the surface of the plug that had been ejected. Photographs of the hole and plug for a typical NASA Flat penetrating shot are shown in figure 17.

Figure 17. Hole and Plug for a Typical Penetrating NASA Flat Projectile Used in the Friction and Mass Study (All photographs show the impacted face of the plate.)

With reference to the results for the straight projectiles in figure 15, note that there are two projectile designs for the 37.5-g mass, one was steel and the other was titanium. The purpose of having two designs was to examine whether the projectile material had any influence on the ballistic characteristics of this projectile/target combination. The data for projectiles 3 and 3a appeared to follow a similar trend, which suggests that, in this case, the material was not a significant factor in the ballistic behavior.

The data for the lightest of the straight projectiles (12.5-g mass) includes several shots for which the final velocity was much lower than expected on the basis of the other five shots in which target penetration was observed. Reexamination of the data confirms that the initial and final speeds were correctly calculated and reported.

Data for the stepped projectiles showed a more consistent trend between final and initial speeds, with only one small deviation from an otherwise monotonic increase in final speed with increasing initial speed for all four projectile masses.

To compare the straight versus the stepped projectiles under similar conditions (the same nominal mass and range of speeds), plots of final versus initial speed for each mass are provided separately in figures 18 through 21.

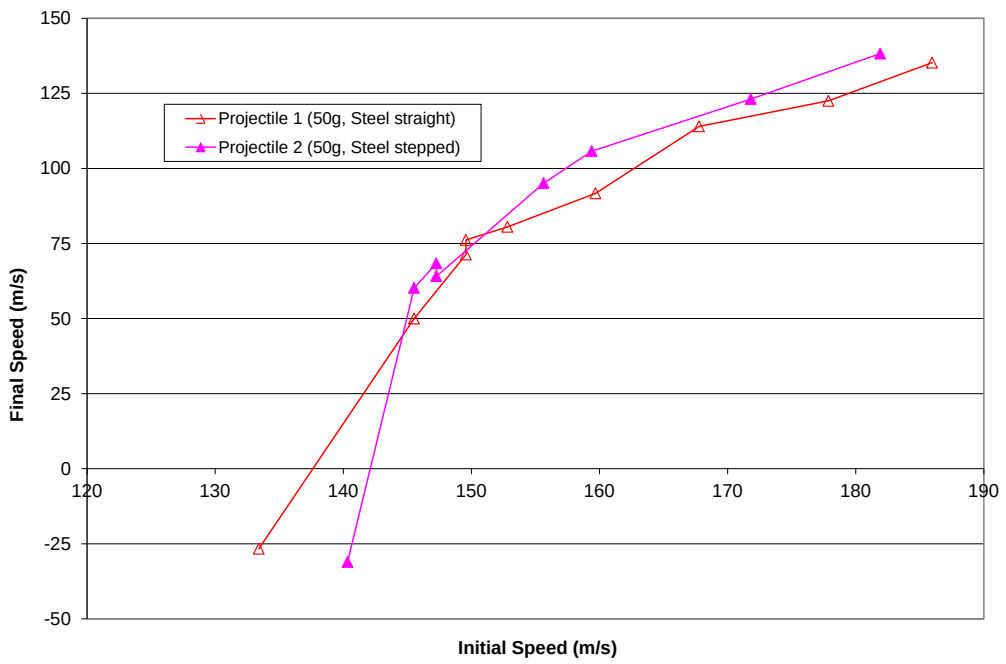

Figure 18. Final vs. Initial Projectile Speeds for 50-g NASA Flat Projectiles Impacting 6.35-mm-Thick Aluminum Plate

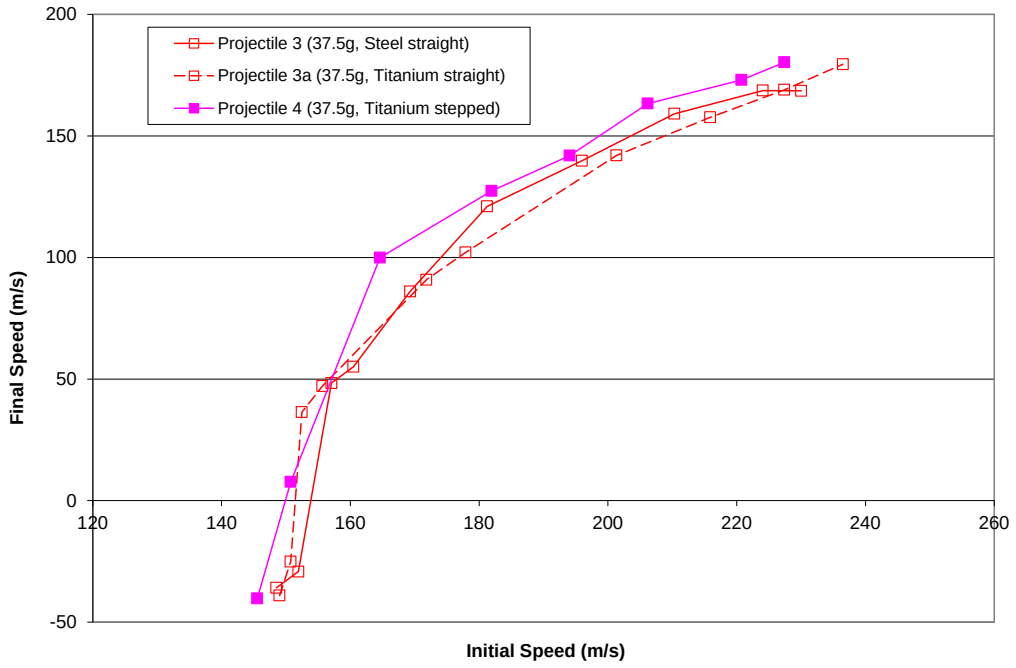

Figure 19. Final vs. Initial Projectile Speeds for 37.5-g NASA Flat Projectiles Impacting 6.35-mm-Thick Aluminum Plate

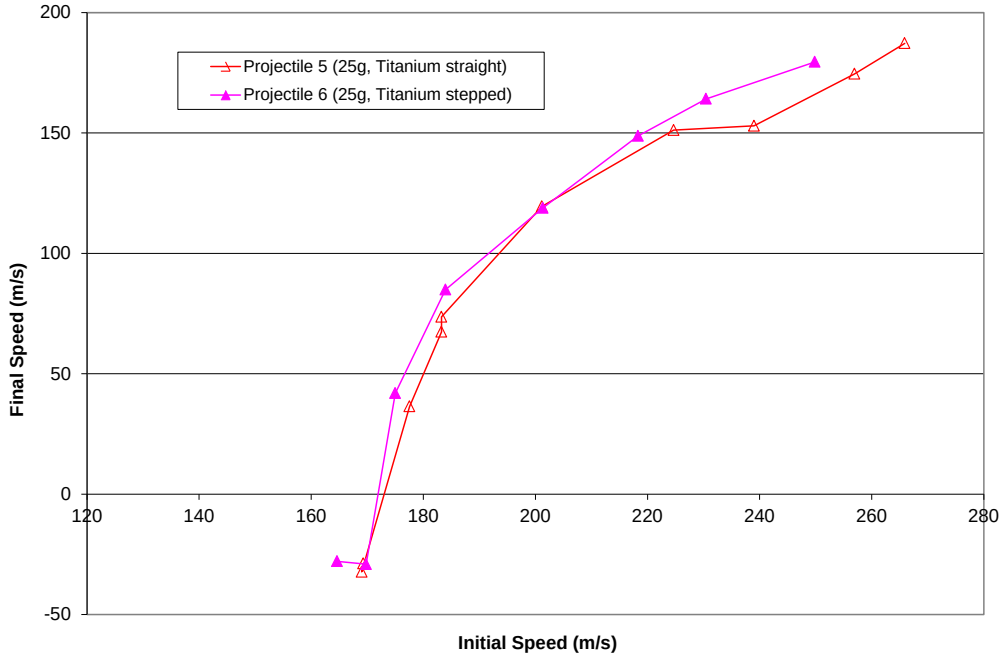

Figure 20. Final vs. Initial Projectile Speeds for 25-g NASA Flat Projectiles Impacting 6.35-mm-Thick Aluminum Plate

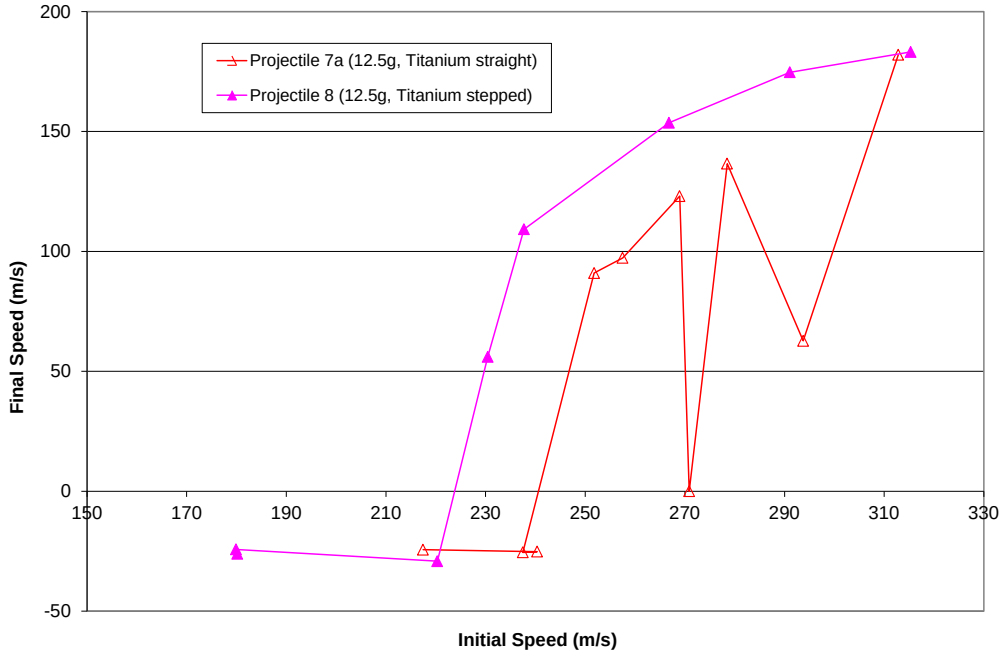

Figure 21. Final vs. Initial Projectile Speeds for 12.5-g NASA Flat Projectiles Impacting 6.35-mm-Thick Aluminum Plate

Figure 22 shows the results for final speed versus initial speed for straight and stepped 37.5-g projectiles with hemispherically tipped ends. The hemispherically tipped projectile impact end produced significantly different results than the NASA Flat projectile impact surface. Comparing the results of all of the 37.5-g projectiles shows that the ballistic limit for the NASA Flat projectiles was approximately 150 m/s, while for the hemispherically tipped projectile, the ballistic limit was between 180 and 200 m/s. This increase in ballistic limit was associated with a substantial increase in the energy that was absorbed by the target plate under hemispherically tipped projectile penetration.

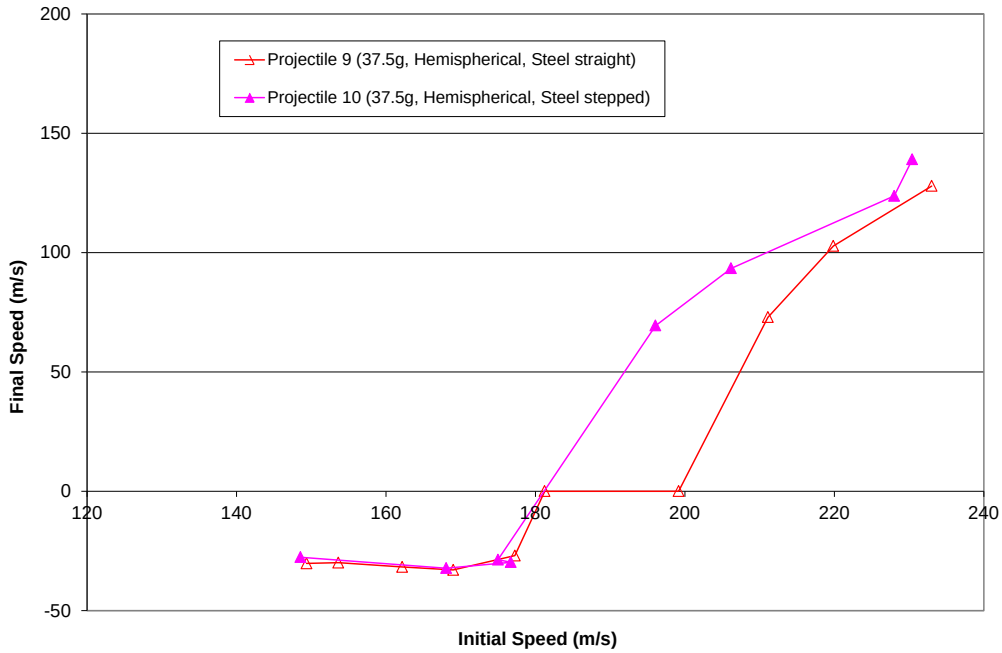

Figure 22. Final vs. Initial Projectile Speeds for 37.5-g Hemispherically Tipped Projectiles Impacting 6.35-mm-Thick Aluminum Plate

The damage caused in the target plate due to a penetrating hemispherically tipped projectile was somewhat different than that observed with the NASA Flat projectiles. In the case of the hemispherically tipped projectiles, a plug was created, but the mass of the plug was about 25% less than the plugs created by penetration of the NASA Flat projectiles. The sides of the target plugs produced by both style projectiles had a similar rough surface, and the shape of the impacting end of the projectile was impressed upon the face of the plug. Similarly, the plug tapered from the impacting face to the exit face, and the interior surface of the hole that was created had been polished by the projectile as it passed through the material. However, the diameter of the plug that resulted from the hemispherically tipped projectile was always less than the 12.7-mm diameter of the projectile. For the projectile to penetrate the target, more material must be deformed by the projectile itself as it passes through the target. In this case, this resulted in considerable cracking of the hole edges on the exit face, and some evidence of interior cracking as well. The plate itself exhibited more out-of-plane macroscopic deformation as a result of the hemispherically tipped projectile impact compared to the NASA Flat projectile impact. The plug and hole for a typical hemispherically tipped projectile are shown in figure 23.

(a) Inlet View (b) Exit View

Figure 23. The Hole and Plug Associated With a Typical Hemispherically Tipped Projectile Impacting 6.35-mm-Thick Aluminum Plate

Figure 24 shows a comparison of the plugs resulting from the penetration of the two tip shapes, along with a projectile that had not been used in the tests. For reference, the mass of the plug created by the NASA Flat projectile was 2.0 g, while the mass plug created by the hemispherically tipped projectile was 1.4 g. An upper bound on the mass of the plugs can be obtained by considering a right circular cylinder of 2024 aluminum (with an assumed density of 2780 kg/m3), which would have a mass of 2.24 g.

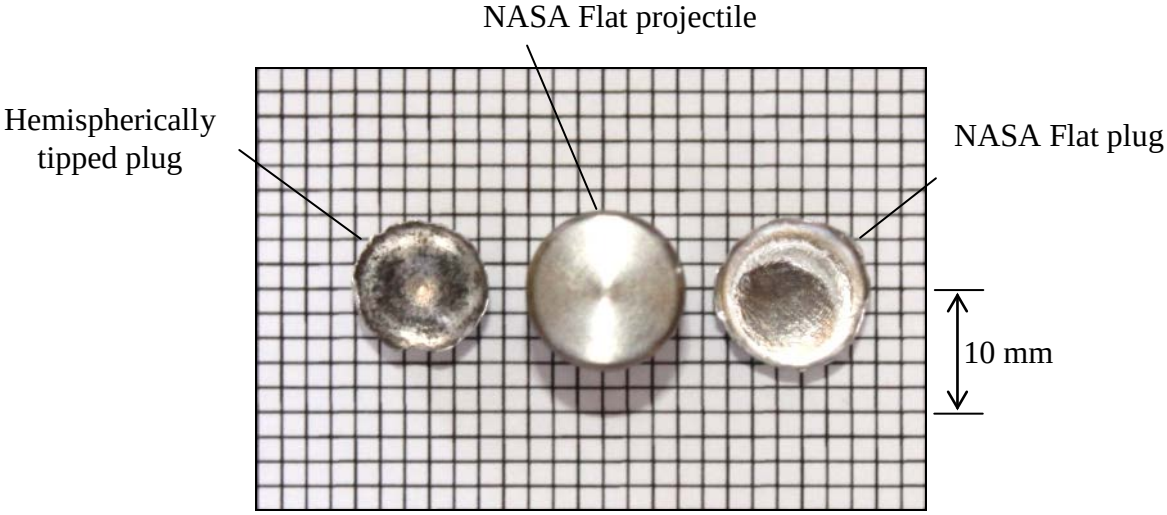

Figure 24. Plugs From Penetration of a Hemispherically Tipped (left) and a NASA Flat (right) Projectile With an Unused NASA Flat Projectile (center) Impacting 6.35-mm-Thick Aluminum Plate

3.1.2 Absorbed Energy.

The main purpose of the friction and mass study was to examine the difference in energy absorbed between the straight and the stepped projectiles and between projectiles of varying mass. Because there is a substantial difference in the length of the full-diameter region between

these two types of projectiles, it was expected that there would be a measurable difference in the energy absorbed between them as well. The straight projectiles present the maximum frictional loss (the full 50.8-mm length of the projectile must pass through and be in contact with the hole created by the impacting tip), while the stepped projectiles represent the minimum frictional loss (only 6.35 mm of the sides of the stepped projectiles are in contact with the sides of the hole as the projectile penetrates).

In this report, the absorbed energy is defined as the difference between the kinetic energy of the projectile before it impacts the target (the initial energy) and the sum of the projectile's final energy (after penetration) and the kinetic energy of the plug.

$$E_{absorbed} = \frac{1}{2} m_{proj} v^2_{proj,initial} - \left(\frac{1}{2} m_{proj} v^2_{proj,final} + \frac{1}{2} m_{plug} v^2_{plug} \right) \tag{1}$$

where

m = mass
v = velocity

Figures 25 and 26 show the absorbed energy versus initial projectile energy for the straight projectiles and for the stepped projectiles, respectively. The data show no clear trend relating absorbed energy to projectile mass beyond the observation that the energy required for initial penetration appears to increase with increasing mass. Once the initial projectile speed was well above the ballistic limit, there was no obvious correlation between absorbed energy and mass.

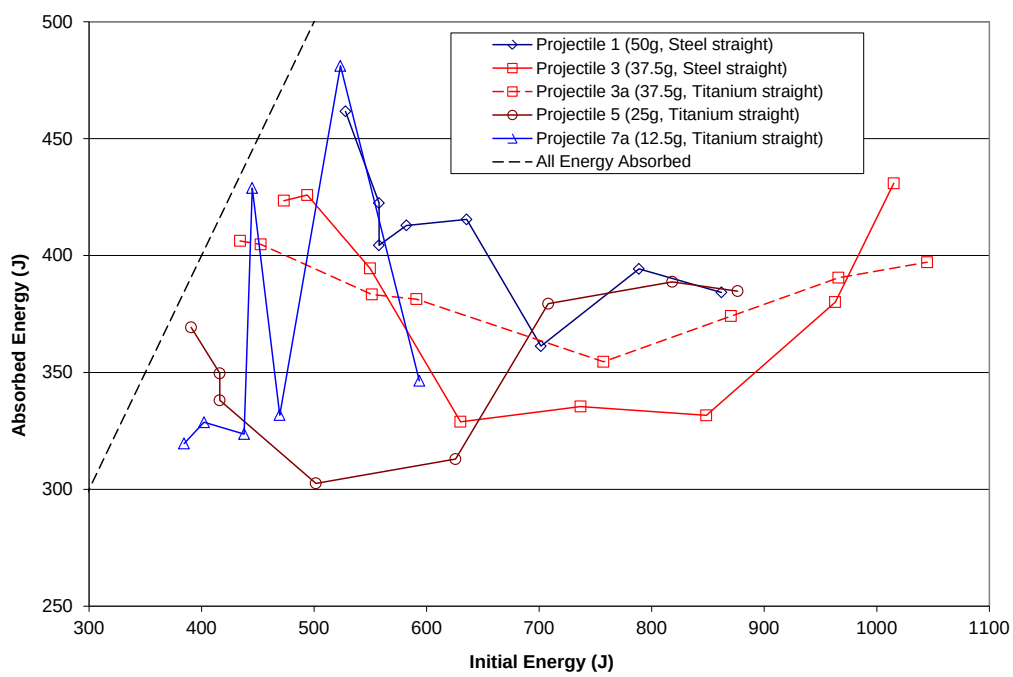

Figure 25. Absorbed vs. Initial Energy for Straight NASA Flat Projectiles Impacting 6.35-mm-Thick Aluminum Plate

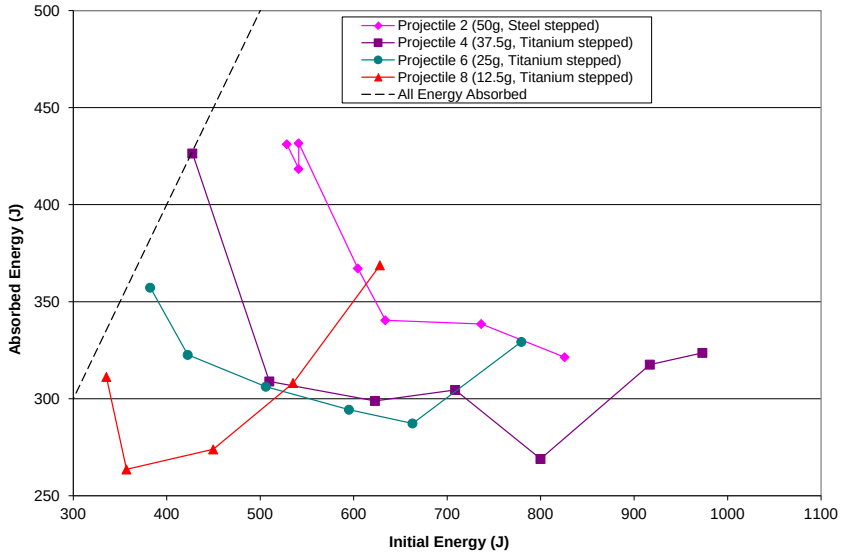

Figure 26. Absorbed vs. Initial Energy for Stepped NASA Flat Projectiles Impacting 6.35-mm-Thick Aluminum Plate

To examine the effect of projectile length (straight versus stepped), it is useful to view the data for each mass separately. Figures 27 through 30 provide this information for the NASA Flat projectiles. In these figures, the error bars indicate the estimated uncertainty based on the measurement errors (projectile velocities, plug velocity, projectile mass, and plug mass). A similar plot for the absorbed energy for the hemispherically tipped projectiles is shown in figure 31.

In general, it appears that the stepped projectiles lost less energy than the equivalent straight projectiles, but the size of the error bars and the overall variation in absorbed energy with initial energy suggests that a more careful analysis of the results is needed to better quantify the effect.

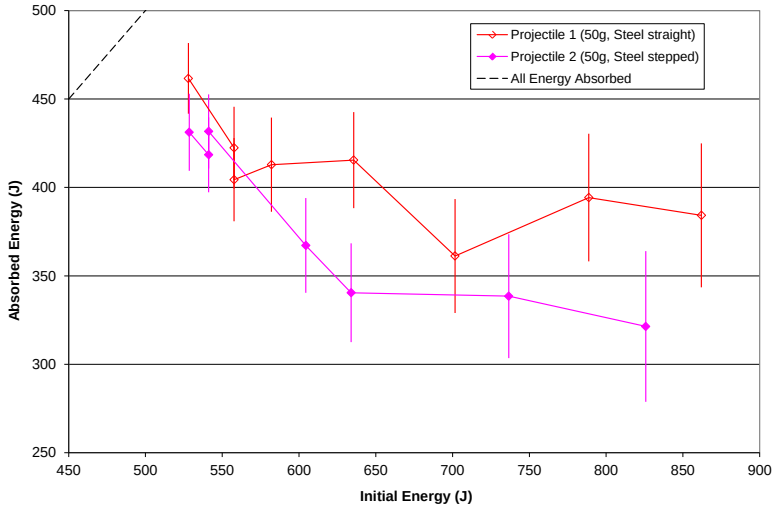

Figure 27. Absorbed vs. Initial Energy for 50-g NASA Flat Projectiles Impacting 6.35-mm-Thick Aluminum Plate

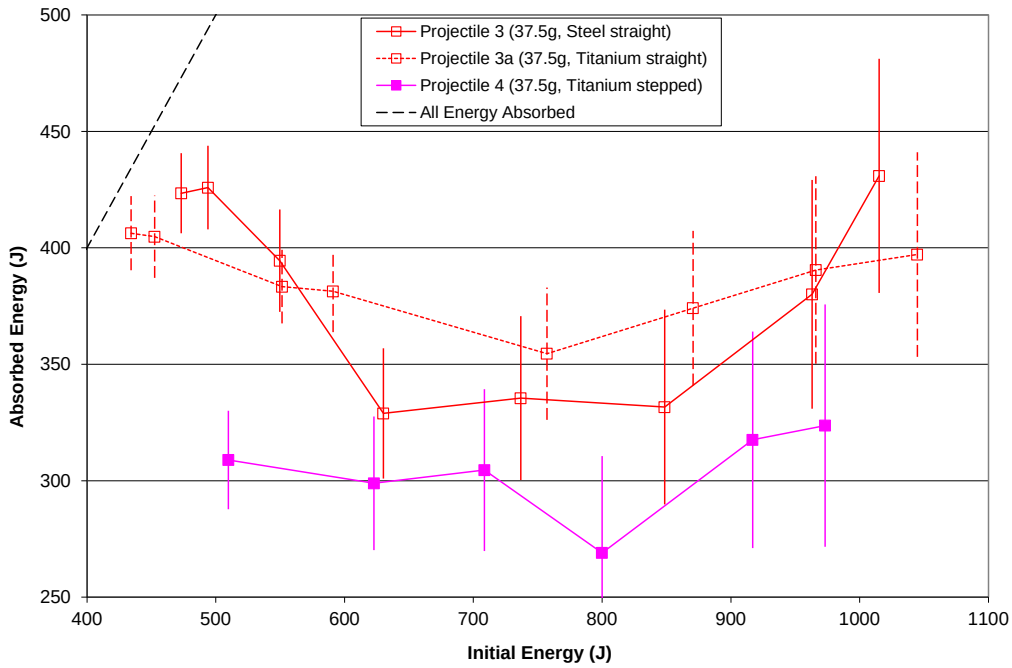

Figure 28. Absorbed vs. Initial Energy for 37.5-g NASA Flat Projectiles Impacting 6.35-mm-Thick Aluminum Plate

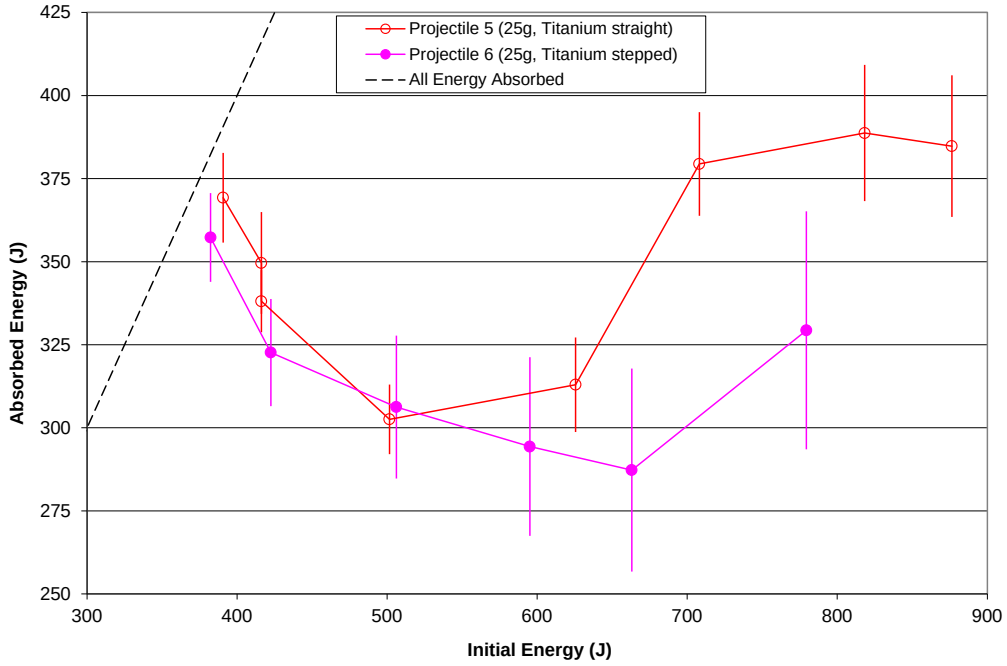

Figure 29. Absorbed vs. Initial Energy for 25-g NASA Flat Projectiles Impacting 6.35-mm-Thick Aluminum Plate

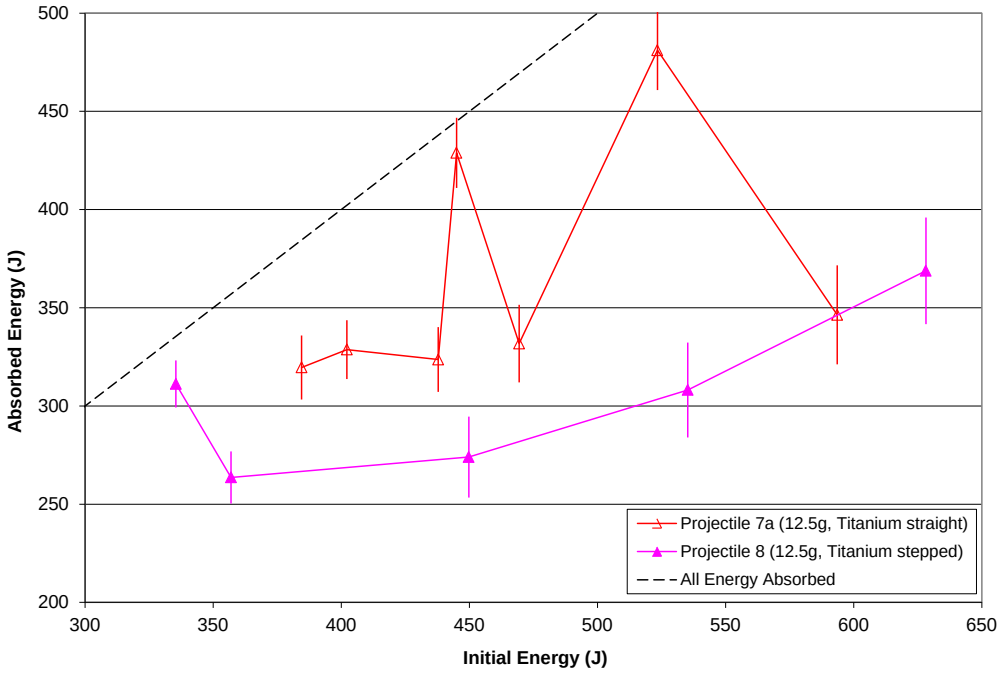

Figure 30. Absorbed vs. Initial Energy for 12.5-g NASA Flat Projectiles Impacting 6.35-mm-Thick Aluminum Plate

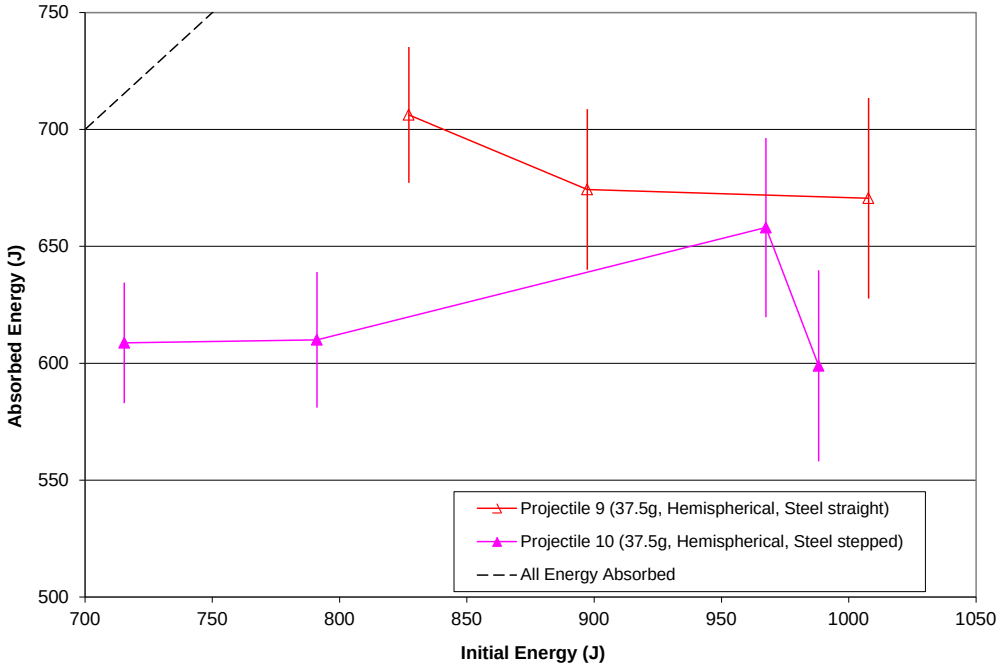

Figure 31. Absorbed vs. Initial Energy for 37.5-g Hemispherically Tipped Projectiles Impacting 6.35-mm-Thick Aluminum Plate

3.1.3 Data Analysis.

The analysis of the data shown in the preceding section was performed to examine the significance of the effects of factors, such as material used to make the projectiles, shape of the projectiles (stepped versus straight), and mass of the projectiles. The statistical software package R [3] was used to perform the analyses shown in the following sections. Details of the code input and results are given in appendix C for each case considered.

3.1.3.1 Effect of Projectile Material.

To achieve the desired mass for each projectile shape, two materials were used: steel for the heavier projectiles and titanium for the lighter projectiles. Given the differences in surface characteristics and hardness between the two materials, it was important to examine whether there was a difference in their ballistic characteristics. The one case in which data were taken for both materials was for the straight NASA Flat projectiles with 37.5-g mass (see figure 28). Focusing on the two sets of straight projectiles (labeled "Projectile 3" for steel and "Projectile 3a" for titanium), two approaches were taken to show that there is no statistically significant difference between the ballistic characteristics of these materials. First, a standard, two-sample *t*-test comparing the data sets provided a significance of $p = 0.764$. This clearly shows that the difference between the means of the absorbed energy for the two data sets, 381.3 J for steel and 386.4 J for titanium, cannot be ascribed to anything other than chance.

An alternative approach is to perform a least-squares fit of the data using the material as a factor. In this approach, a quadratic relation[1] between the absorbed energy (A) and the initial energy (E) is used.

$$A = a + bE + cE^2 + \delta_m \tag{2}$$

where a represents the intercept of the data and δ_m represents the difference between the results for steel versus titanium. The coefficients for this data fit are given in table 3. The quadratic fit of absorbed energy with initial energy was found to be highly significant, but there was no significant difference between the data for the steel and the titanium projectiles ($p = 0.774$). Therefore, it was concluded that the steel and titanium projectiles were sufficiently similar in their ballistic characteristics for this target and that the projectile material would not be considered in the subsequent analysis of the full set of data.

[1] There is no physical reason to choose a quadratic relationship between initial and absorbed energy. This form is used only because the involved data suggests that this function may provide a good empirical fit.

Table 3. Coefficients of Fit of Equation 2 to Data From 37.5-g Straight NASA Flat Projectiles Comparing Projectile 3 (Steel) to Projectile 3a (Titanium)

Coefficient	Units	Estimate	Standard Error	Significance
a	J	811.3	84.4	5.46E-7
b	--	-1.235	0.243	0.00027
c	1/J	0.000823	0.000165	0.00031
δ_m (titanium)	J	0	--	--
δ_m (steel)	J	3.01	10.3	0.774
Adjusted R^2	--	0.610	--	--

3.1.3.2 Effect of Projectile Shape and Mass.

In assessing whether the data show an effect on absorbed energy due to projectile shape, again, two approaches were taken: a standard two-sample *t*-test and a least-squares data fitting. An implicit assumption in the *t*-test was that the data did not depend on any other variable (initial energy, mass, or material). The means and standard deviations for the absorbed energy of all the penetrating shots are given in table 4. There were more test shots performed for the straight projectiles, partly because two materials were used for the 37.5-g projectiles. The difference in the means was 46 J, which was roughly equal to the standard deviations associated with the two data sets. However, when the *t*-test was performed, it showed a significance of p = 0.000169, which strongly suggested that the difference in the means was not simply due to chance.

Table 4. Statistics for all Straight and Stepped Projectiles With the NASA Flat Tip

Shape	Test Shot No.	Absorbed Energy of Penetrating Shots	
		Mean (J)	Standard Deviation (J)
Straight	39	379	41.9
Stepped	25	333	49.7

The alternative approach involving a least-squares fit of the data involved a function that was taken to be linear in the projectile mass (m) and, again, quadratic in the initial energy[2].

$$A = a + bE + cE^2 \; d \; m + \delta_{shape} \tag{3}$$

where δ_{shape} represents the difference between the results for the straight projectiles versus those for the stepped projectiles. The coefficients for this data fit are given in table 5.

[2] There is no physical reason to use this particular functional form. It was chosen empirically.

Table 5. Coefficients of Fit of Equation 3 to Data From All NASA Flat Projectiles Comparing Stepped Projectiles to Straight Projectiles

Coefficient	Units	Estimate	Standard Error	Significance
a	J	377	67	5.01E-7
b	--	-0.30	0.22	0.174
c	1/J	1.85E-4	1.6E-4	0.248
d	J/g	1.96	0.44	4.64E-5
δ_{shape} (stepped)	J	0	--	--
δ_{shape} (straight)	J	46.9	10.3	2.77E-5
Adjusted R^2	--	0.362	--	--

The difference associated with the shape factor was, naturally, close to the difference between the means of all straight and all stepped projectiles (δ_{shape} = 46.9 J), and it was shown to be highly significant (p = 0.0000277). Thus, it was highly unlikely that this difference was simply due to chance.

This data fit also suggested that the absorbed energy depended on projectile mass as well. On average, the more massive the projectile, the more energy was absorbed as the projectile created the plug and penetrated the plate.

The 37.5-g hemispherically tipped projectiles (see figure 31) were considered. The means and standard deviations for the absorbed energy of all penetrating shots using hemispherically tipped projectiles are given in table 6. The difference in the means is 65 J, which is considerably greater than the standard deviations associated with the two data sets. When the *t*-test was performed, it showed a significance of p = 0.0165, which suggested that the difference in the means was not simply due to chance.

Table 6. Statistics for All Straight and Stepped Projectiles With Hemispherical Tip

Shape	Test Shot No.	Absorbed Energy of Penetrating Shots	
		Mean (J)	Standard Deviation (J)
Straight	3	684	19.4
Stepped	4	619	26.5

The results shown in figures 25 and 26 suggested some dependence of absorbed energy on projectile mass. The statistical analysis associated with the assumed fit of energy to mass and projectile shape, equation 3, confirms that this dependence is significant. Another way to examine the relationship between mass and absorbed energy is to consider the energy absorbed at the ballistic limit, since the data in figures 25 and 26 showed that the effect of mass appeared to be greatest near the ballistic limit. To do this, using the figures in section 3.1.1, the ballistic limit was estimated from the final velocity versus initial velocity data to be the zero crossing of the straight line segment joining the last shot that rebounded from the target and the first shot

that fully penetrated. The energy of the projectile at the ballistic limit was then calculated, and error bars were assigned assuming that the ballistic limit was known to within ±5 m/s.

Figure 32 shows the variation of initial projectile energy at the ballistic limit versus projectile mass for the four masses with NASA Flat tips and stepped sides. A straight-line fit to the four points on this plot provides a visual indication of the strong dependence of the projectile energy at the ballistic limit on projectile mass. The slope of this line corresponds to the coefficient *d* in equation 3, although the value of *d* given in table 5 involves all the data, not just that near the ballistic limit. As a result, the value of *d* in table 5 is somewhat smaller than the slope of the line in figure 32.

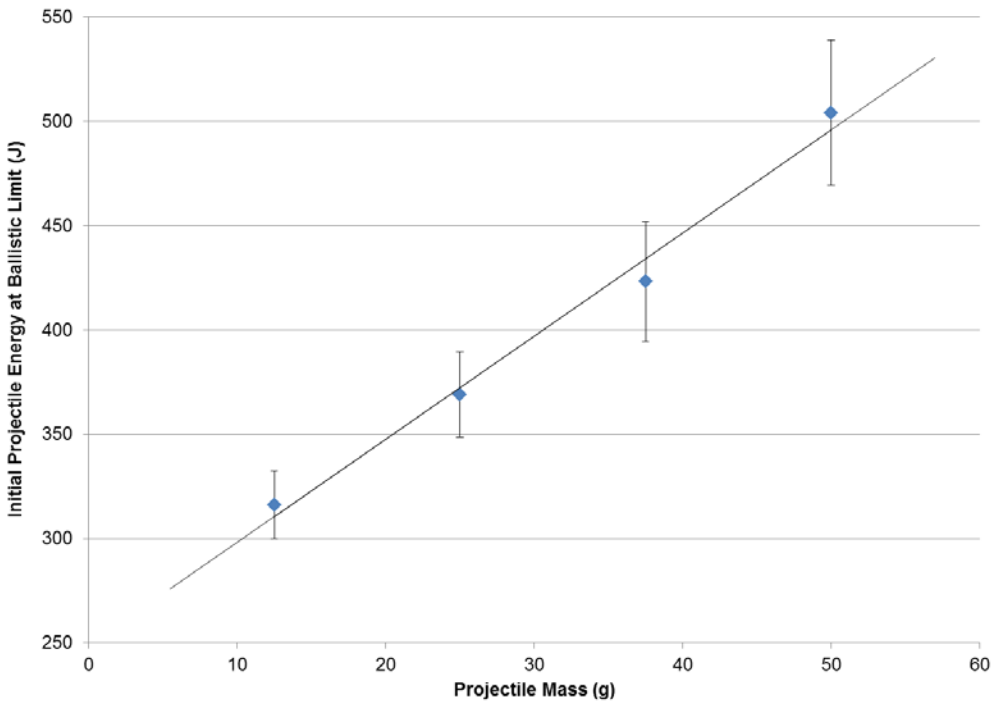

Figure 32. Initial Projectile Energy at the Ballistic Limit vs. Mass for Stepped Projectiles With NASA Flat Tips Impacting 6.35-mm-Thick Aluminum Plate

3.2 THE NASA ALUMINUM STUDY.

This section provides details on independent measurements of projectile penetration of the same lot of 2024 aluminum that was previously tested at the NASA-GRC and OSU under other FAA grants. Tests were performed using both NASA Flat and hemispherically tipped projectiles with a 12.7-mm diameter.

Results show a variety of failure modes, including shear plug failure for NASA Flat projectiles penetrating the 3.18-mm-thick sheet, petaling for hemispherically tipped projectiles penetrating the sheet material, and fragmentation of the target material for tests involving both projectile types for the thicker (6.35- and 12.7-mm) plates.

3.2.1 Final vs. Initial Projectile Speed.

Figures 33 and 34 show the final projectile speed versus the initial projectile speed for the NASA Flat and hemispherically tipped projectiles, respectively, impacting the NASA aluminum targets of varying thickness. To more clearly see the differences between the NASA Flat and the hemispherically tipped projectiles, the same data are shown for the 3.18- and 6.35-mm plate thicknesses in figures 35 and 36, respectively. Three NASA Flat projectiles experienced large rotation upon penetration through the target for the 3.18-mm sheet causing a larger than normal plug. The data associated with these projectiles are identified in figures 33 and 35 by the solid-filled data markers. The complete set of data is provided in appendix B.

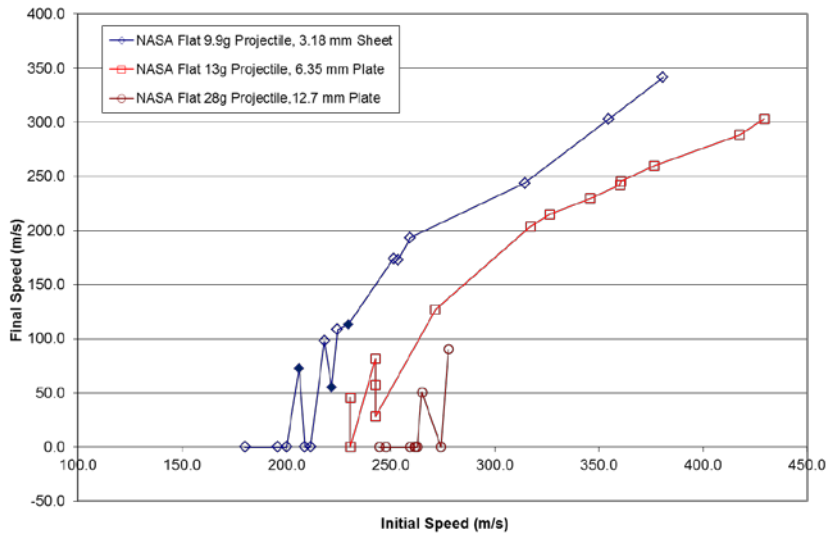

Figure 33. Final vs. Initial Speed for NASA Flat Projectiles Impacting NASA Aluminum Targets

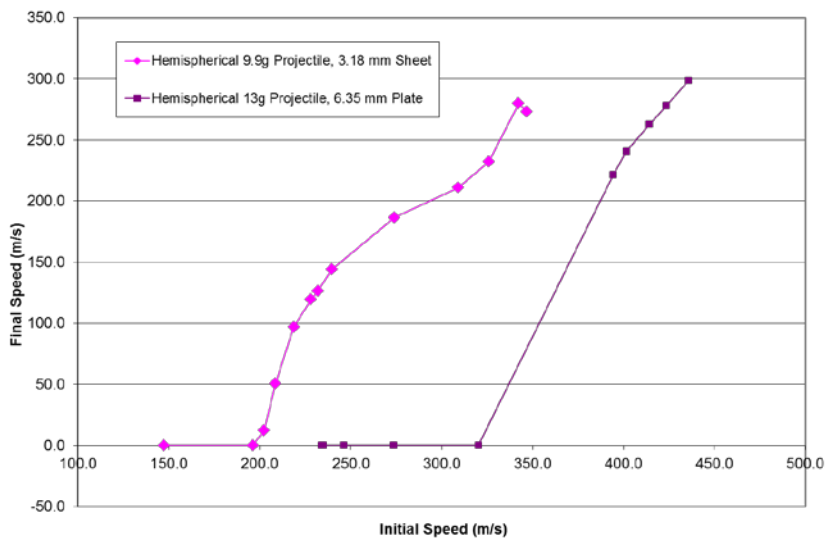

Figure 34. Final vs. Initial Speed for Hemispherically Tipped Projectiles Impacting NASA Aluminum Targets

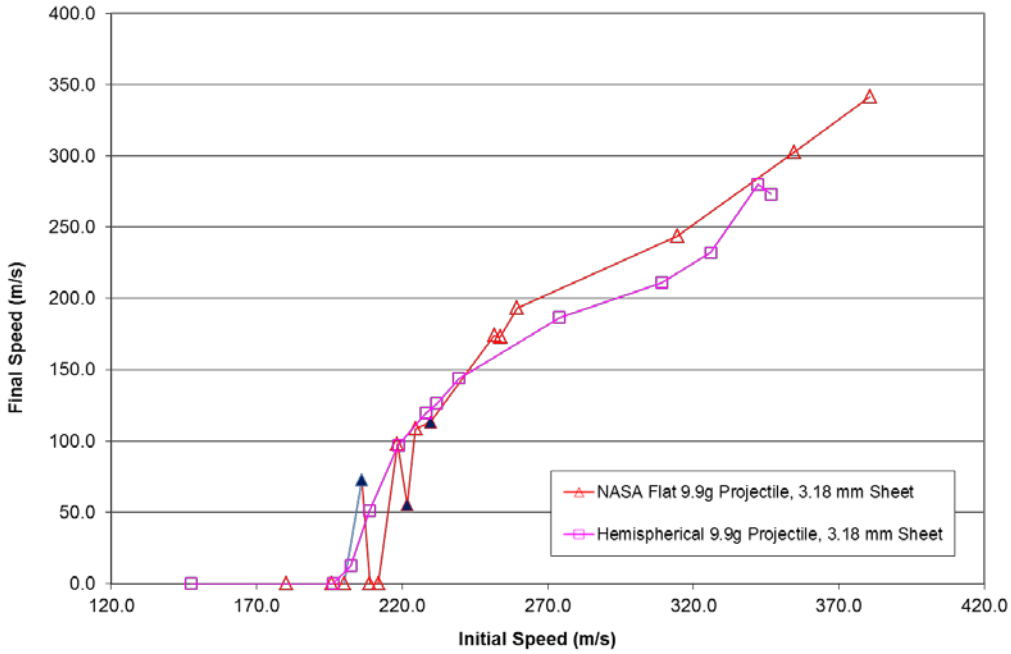

Figure 35. Final vs. Initial Speed for NASA Flat and Hemispherically Tipped Impacting Projectiles 3.18-mm-Thick NASA Aluminum Targets

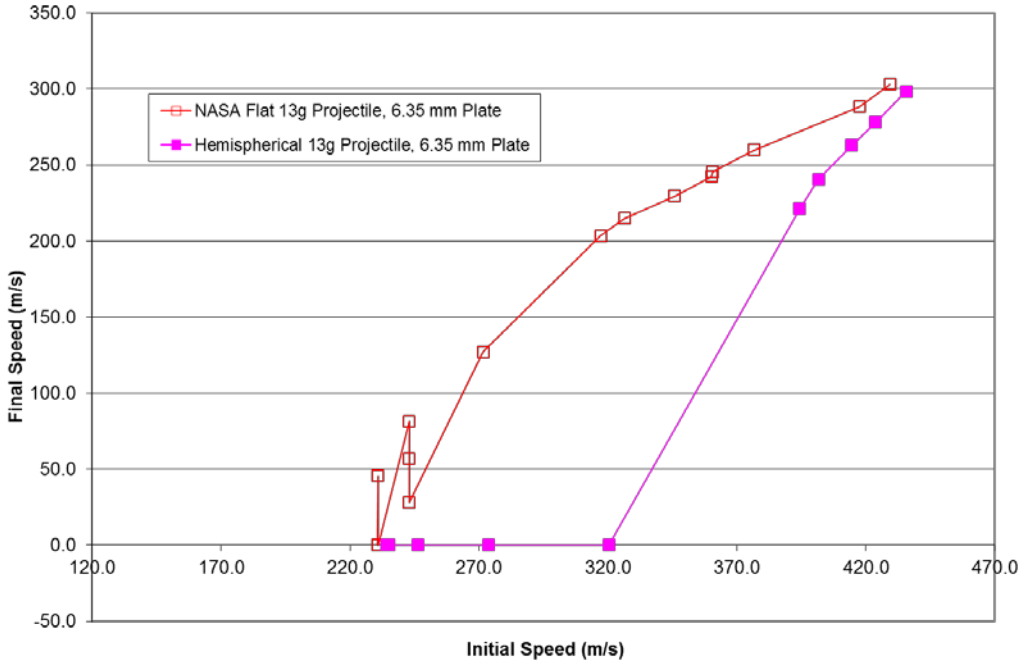

Figure 36. Initial vs. Final Speed for NASA Flat and Hemispherically Tipped Impacting Projectiles 6.35-mm-Thick NASA Aluminum Targets

3.2.2 Nature of Damage.

The nature of the damage to the plate depends on a variety of factors, including the thickness of the plate, the tip shape of the projectiles, the speed of impact, and the projectile orientation on impact. Broadly characterized, the difference is associated with the extent to which the edges of the hole tear as the projectile passes through it and the number and size of the fragments that are created. In all cases, a central plug was ejected prior to the projectile passing through the plate. As with the tests for the friction and mass study, the edges of the plug were not completely smooth, and the shape of the plug was not a perfect right circular cylinder. Rather, the diameter of the plug was somewhat larger at the impacting face than at the exit face. Additionally, a number of the tests showed fragments of a variety of sizes following the main plug. For the purpose of the damage description, each material thickness is addressed separately.

The 3.18-mm 2024-T3 sheet exhibited two distinct failure modes when impacted by the NASA Flat projectiles. If the projectile hit with relatively little rotation, a clean shear plug with a circular cross section was produced. However, for three shots at speeds near the ballistic limit, the projectile rotated by such a significant amount that the hole produced was not circular, but more of a figure-eight shape. The larger portion of the hole was created by the impacting face, while the smaller portion was created when the flank of the projectile hit the sheet as it rotated. In these cases, both the projectile and the plug tumbled through the field of view of the video. Photographs of the exit hole for typical NASA Flat penetrating shots are shown in figure 37, along with one frame of the video showing the projectiles and plugs. Figure 37(a) and (b) shows one of the figure-eight damage tests associated with substantial projectile rotation, and figure 37(c) and (d) shows the standard circular plug and relatively little projectile rotation.

Hemispherically tipped projectiles penetrating the 3.18-mm-thick NASA aluminum sheet produced a consistent plug-petal damage pattern. The plugs in these cases were slightly smaller than the circular plugs associated with small-rotation NASA Flat projectiles for the same sheet and were rounded to conform with the hemispherical impacting tip of the projectile. As the shank of the projectile passed through the hole, the sheet cracked or tore in a number of places around the hole forming the petals. There were typically between eight and ten distinct cracks, all radiating outward from the edge of the hole, but of varied lengths. Figure 38 shows the typical damage pattern for a hemispherically tipped projectile penetrating the 3.18-mm-thick sheet.

NASA Flat Test Number 4

(a)

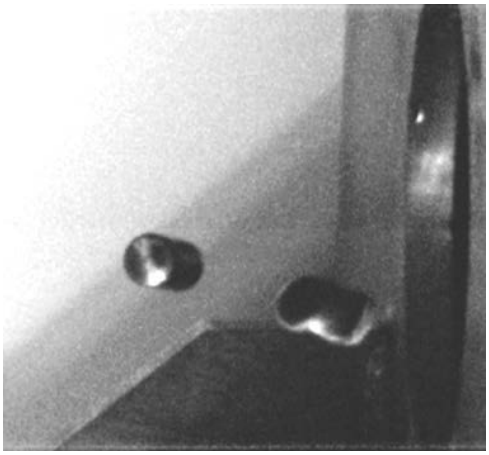

(b)

NASA Flat Test Number 9

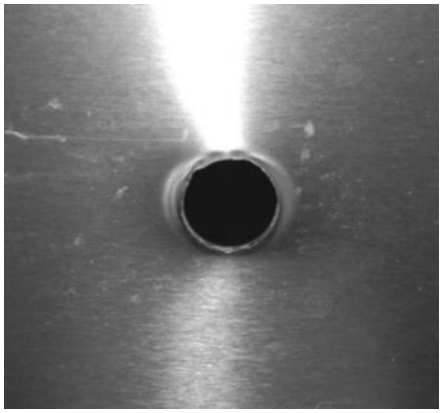

(c)

(d)

Figure 37. Photographs of the Exit Side and One Frame of the Postpenetration Video of 3.18-mm-Thick NASA Aluminum Sheet and NASA Flat Projectiles for Test 4 (a and b) and Test 9 (c and d)

Hemispherical Test Number 10

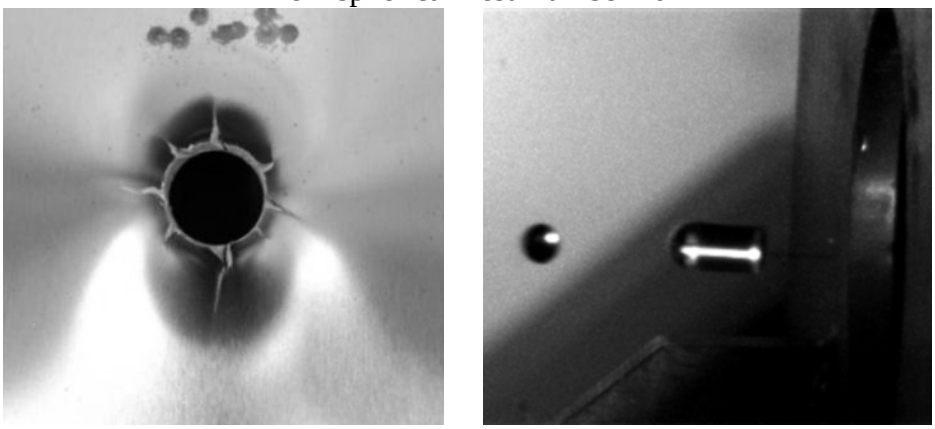

(a) (b)

Figure 38. Photographs of the (a) Exit Side and One Frame of the (b) Postpenetration Video of a Hemispherically Tipped Projectile Penetrating a 3.18-mm-Thick NASA Aluminum Sheet

Penetration of the 6.35-mm-thick NASA 2024-T351 aluminum plate showed some degree of fragmentation of the target material for all tests. In all cases, there was a well-defined central plug, followed by fragments of various sizes, speeds, and exit angles. For the NASA Flat projectiles at relatively low speeds near the ballistic limit, the fragments were small, while for the NASA Flat projectiles at higher speed and the hemispherically tipped projectiles at all speeds, the fragments were more substantial.

Figure 39 shows two representative shots for the NASA Flat projectiles penetrating the 6.35-mm-thick NASA aluminum plate. This figure shows a photograph of the hole taken from the exit side of the plate and a single frame of the video showing the projectile, plug, and fragments after penetration. Test number 10 had an initial speed of 243 m/s, just above the ballistic limit, while test number 21 had an initial speed of 429 m/s. The slower-speed shot shows only a small amount of small fragments immediately behind the plug. The video image from the higher-speed shot shows the larger fragments trailing the projectile. The source of these larger fragments are shown in the photograph of the exit side in figure 39(c) where the edges of the hole broke off as the projectile passed through.

All the hemispherically tipped projectiles penetrating the 6.35-mm-thick NASA aluminum plate exhibited damage similar to that of the high-speed NASA Flat projectiles: a plug was first ejected from the plate, the projectile passed through the hole, and some or all of the petals that form around the hole broke off from the plate and became fragments that trailed the projectile. The fragments tend to move away from the plate more slowly than the projectile and are usually at an angle to the path of the projectile. Figures 40 (hemispherical test number 38) and 41 (hemispherical test number 18) show photographs of the exit side of a typical plate and video images for several hemispherically tipped projectiles. The black arrow in figure 41 shows the path of the plug, the solid-white arrows show the path of the projectile, and the dashed white arrows show the paths of the larger fragments.

NASA Flat Test Number10

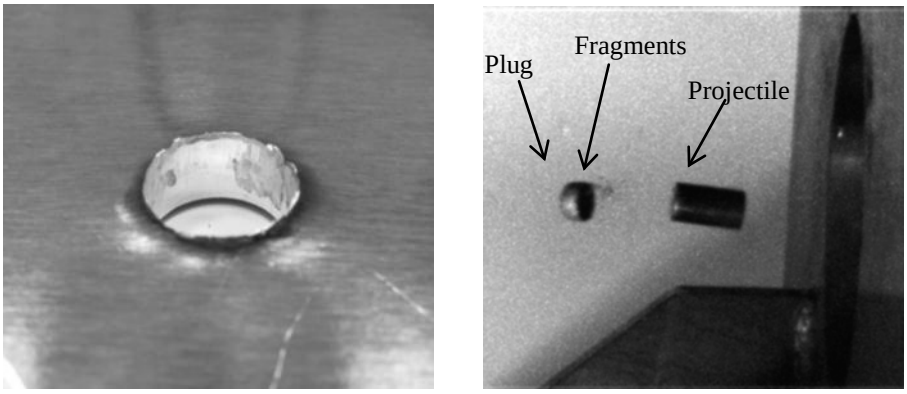

(a) (b)

NASA Flat Test Number 21

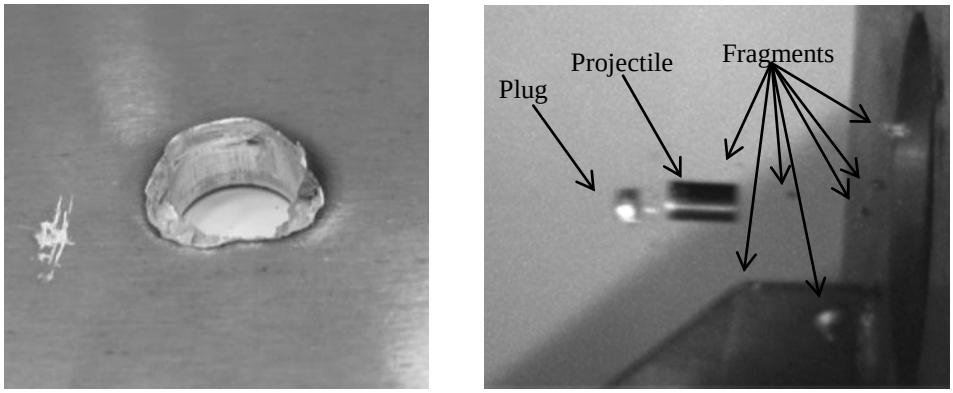

(c) (d)

Figure 39. Photographs of the Exit Side and One Frame of the Postpenetration Video of 6.35-mm-Thick NASA Aluminum Plate and NASA Flat Projectiles

Hemispherical Test Number 38

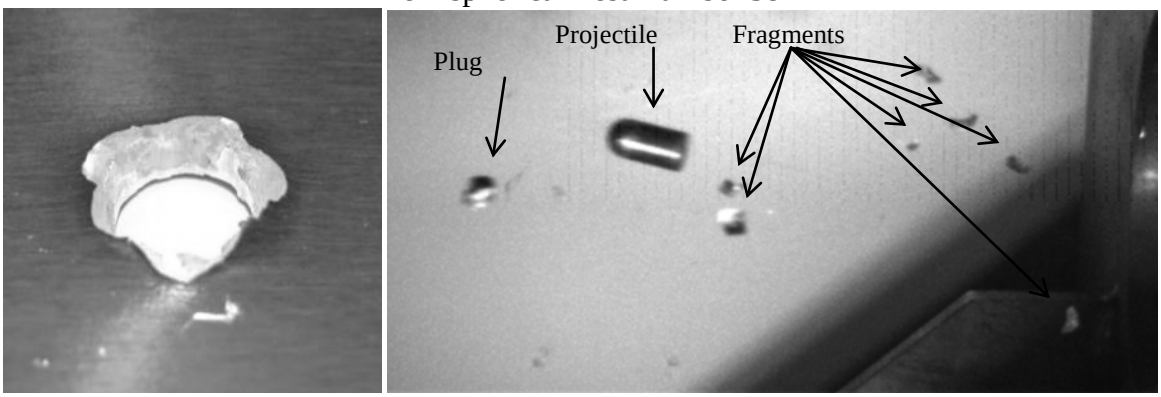

(a) (b)

Figure 40. Photographs of the Exit Side and One Frame of the Postpenetration Video of a Hemispherically Tipped Projectile Penetrating a 6.35-mm-Thick NASA Aluminum Plate

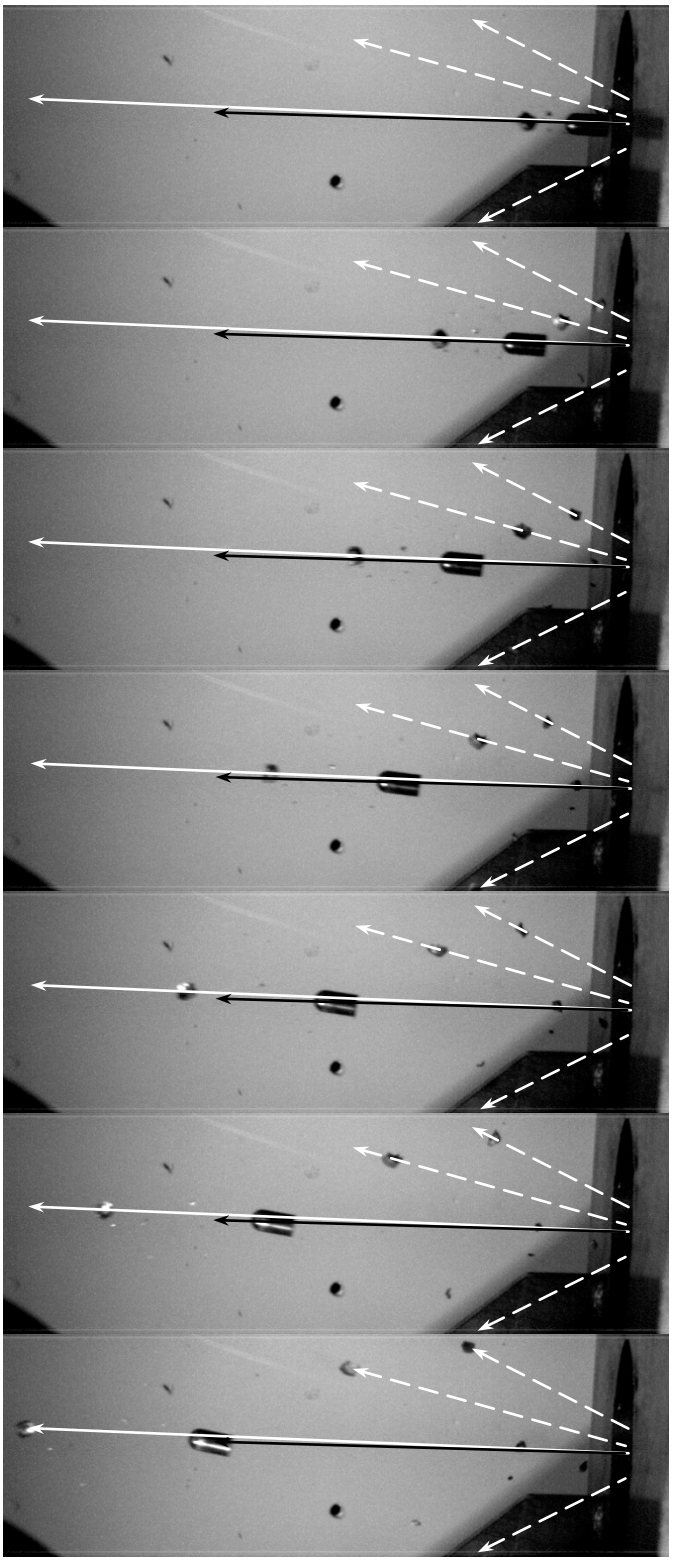

Figure 41. Series of Video Frames of Postpenetration Video of Hemispherically Tipped Projectile Penetrating a 6.35-mm-Thick NASA Aluminum Plate

Penetration of the 12.7-mm-thick NASA 2024-T351 aluminum plate showed some degree of fragmentation of the target material for all tests, even those for which the projectile did not fully penetrate the target. Figure 42 shows the plug, fragment material, and projectile for two tests for the 12.7-mm-thick NASA aluminum targets. Both video images show a substantial cloud of small fragments following the plug. Figure 42 (test number 9) had no projectile penetration of the target.

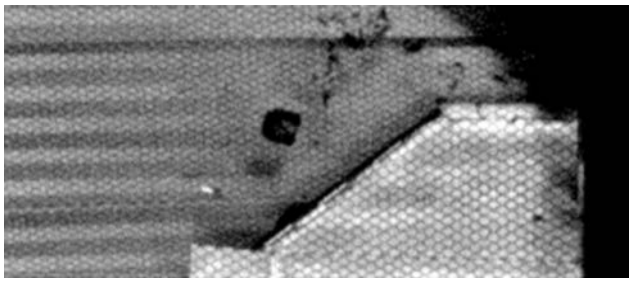

Figure 42. Video Image Showing the Plug and Fragments for Test Number 9, NASA Flat Projectile Impacting 12.7-mm-Thick NASA Aluminum Plate

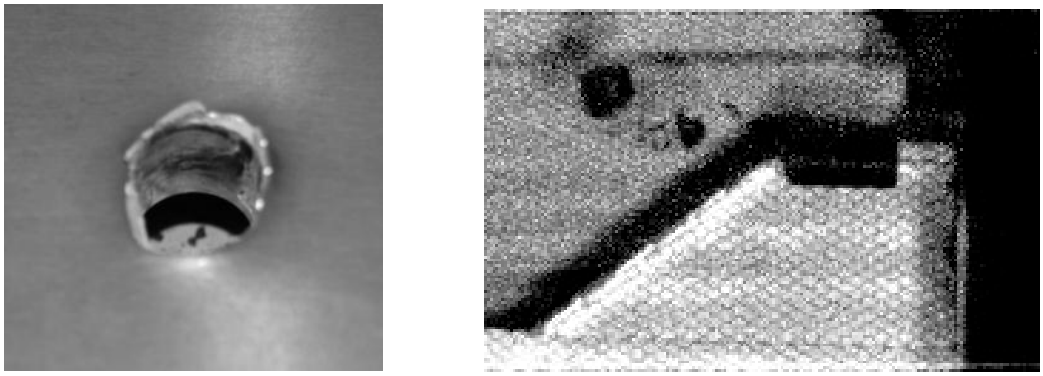

(a) (b)

Figure 43. Photograph of the (a) Exit Side and (b) One Frame of the Postpenetration Video of Test Number 5 of the 12.7-mm-Thick NASA Aluminum Plate Penetrated by a NASA Flat Projectile

3.2.3 Absorbed Energy.

Plots showing the energy absorbed for each test are shown in figures 44 through 48 for the various plate thicknesses and projectile shapes. For the NASA Flat projectiles penetrating the 3.18-mm-thick sheet, the amount of energy absorbed decreased as the initial energy increases beyond the ballistic limit. For the NASA Flat projectiles penetrating the 6.35-mm-thick plate, the amount of energy absorbed increased as the initial energy increased. There was insufficient data to suggest a trend for the postballistic limit energy absorption for the 12.7-mm-thick plate. For the hemispherically tipped projectiles, the absorbed energy did not change significantly beyond the ballistic limit.

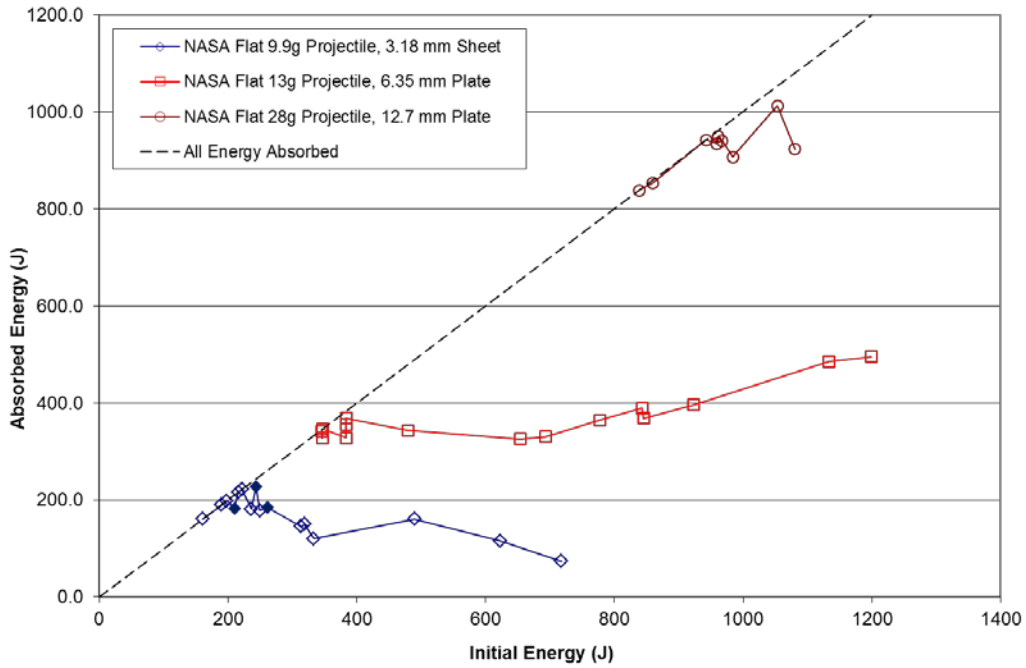

Figure 44. Absorbed Energy for NASA Flat Projectiles Impacting NASA Aluminum Targets

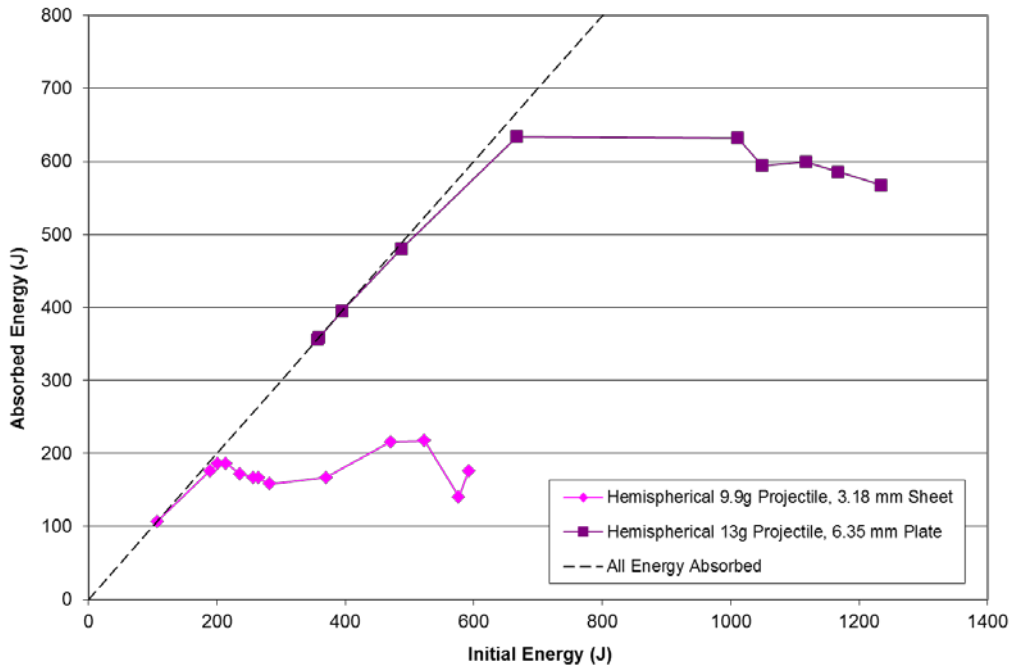

Figure 45. Absorbed Energy for Hemispherically Tipped Projectiles Impacting NASA Aluminum Targets

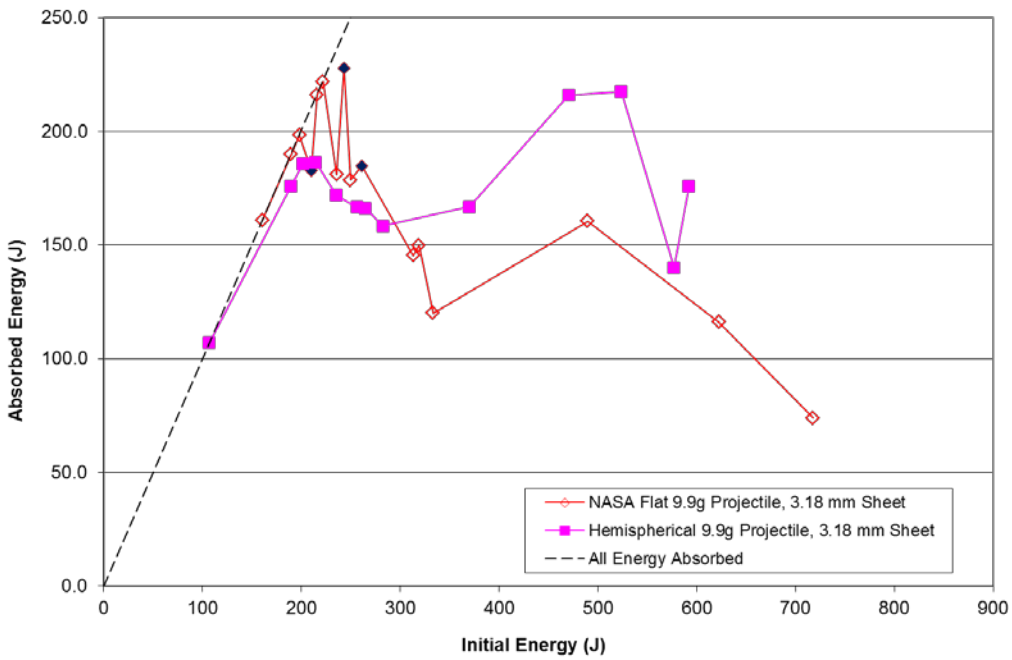

Figure 46. Absorbed Energy for NASA Flat and Hemispherically Tipped Projectiles Impacting 3.18-mm-Thick NASA Aluminum Targets

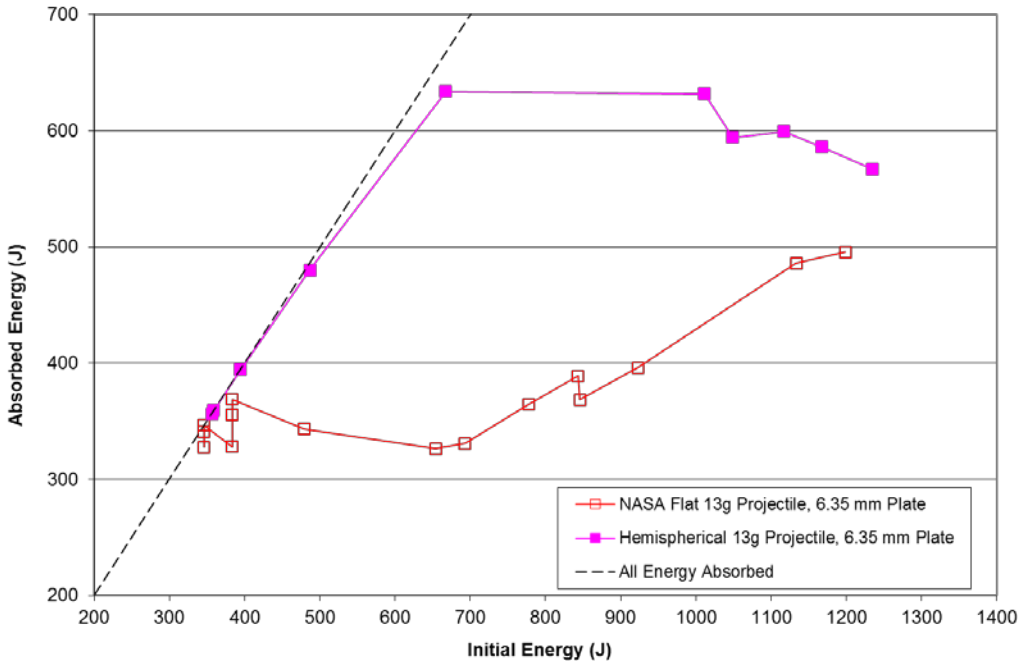

Figure 47. Absorbed Energy for NASA Flat and Hemispherically Tipped Projectiles Impacting 6.35-mm-Thick NASA Aluminum Targets

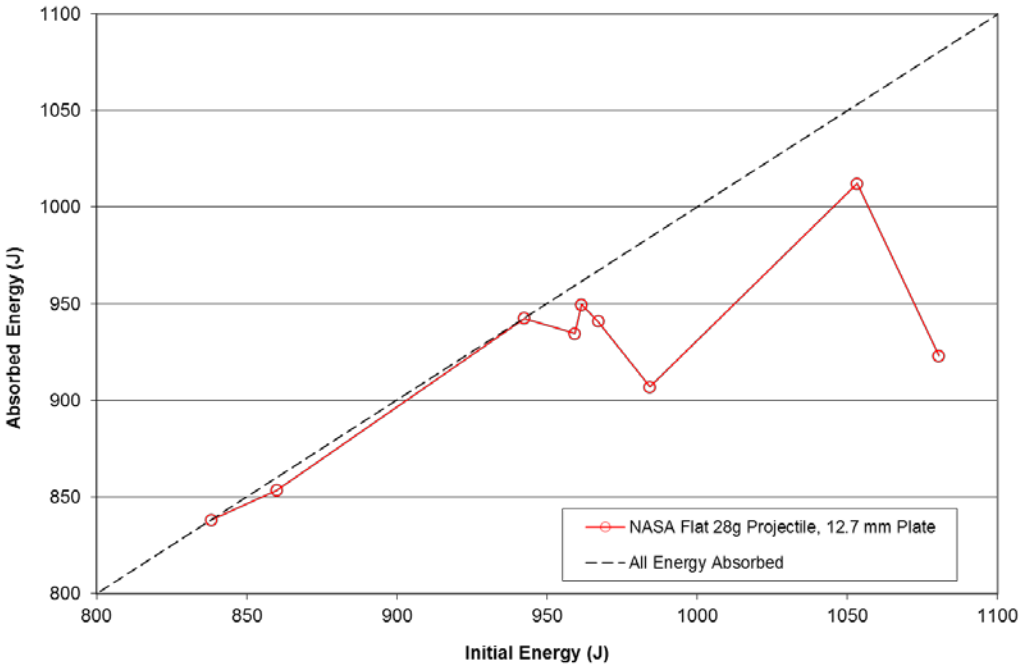

Figure 48. Absorbed Energy for NASA Flat and Hemispherically Tipped Projectiles Impacting 12.7-mm-Thick NASA Aluminum Targets

4. CONCLUSIONS.

This report presents the results of two sets of tests. In the first test set, the friction and mass tests, the goal was to examine the effect of projectile mass, end shape, and effective length on the penetration characteristics of a particular type of target. In these friction and mass tests, all targets were 127-mm-square plates of 6.35-mm-thick material. The second test set examined three thicknesses of material from the same lots as previously tested at National Aeronautics and Space Administration (NASA)-Glenn Research Center and at The Ohio State University. Projectiles used for these tests varied by mass and end shape, but for each material thickness, the goal was to select a projectile mass that would achieve a ballistic limit of approximately 213 m/s (or approximately 700 ft/s).

Results showed that there was no measureable difference between the penetration characteristics of projectiles of the same mass and shape (made of either hardened steel or Grade 5 titanium) impacting 2024 aluminum targets. Projectile mass was significant in terms of absorbed energy near the ballistic limit, with an increase in projectile mass resulting in an increase in the energy required to initially penetrate the target, which shows that penetration is dependent on velocity as well as total energy. This correspondence between absorbed energy and projectile mass did not persist once the initial speed was well above the ballistic limit. The effect of friction was significant, with longer projectiles absorbing more energy during penetration than shorter projectiles. The mode of material failure that led to penetration was strongly dependent on the thickness of the target, the shape of the projectile tip, and the speed at which the projectile impacted the target. In general, hemispherically tipped projectiles caused tearing failures in

thinner targets, flat-ended projectiles caused shear plug failure, and fragmentation occurred at high-impact velocities for the thicker targets.

5. REFERENCES.

1. Donovan, K., Johnson, G., and Zohdi, T., "Impact Tests of Aircraft Aluminums and Composites for Uncontained Engine Fragment Modeling," FAA report DOT/FAA/AR-08/46, October 2008.

2. Phantom High-Speed Digital Imaging by Vision Research, Inc., http://visiblesolutions.com/.

3. R Development Core Team, "R: A Language and Environment for Statistical Computing, R Foundation for Statistical Computing," Vienna, Austria, 2010, ISBN 3-900051-07-0, http://www.R-project.org.

APPENDIX A—MACHINE DRAWINGS FOR PROJECTILES USED IN THE FRICTION AND MASS STUDY

Figures A-1 through A-9 show the mechanical drawings for the National Aeronautics and Space Administration flat impact tip projectiles. Figures A-10 and A-11 show the mechanical drawings for the hemispherical impact tip projectiles. Since these drawings were used for the manufacture of the projectiles, all linear dimensions are given in inches.

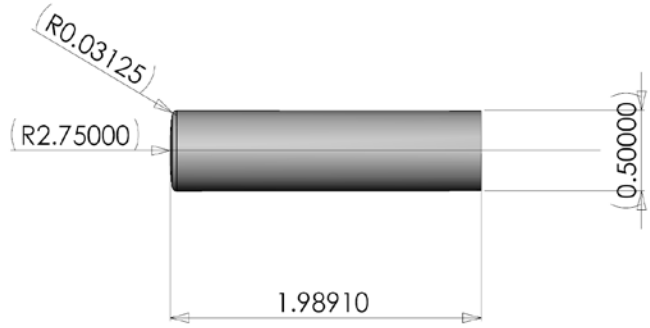

Figure A-1. Projectile 1 (50-g Straight)

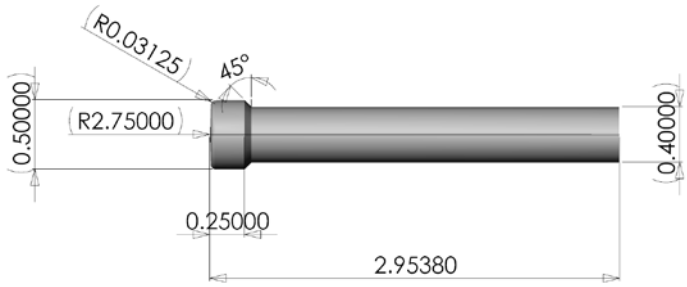

Figure A-2. Projectile 2 (50-g Stepped)

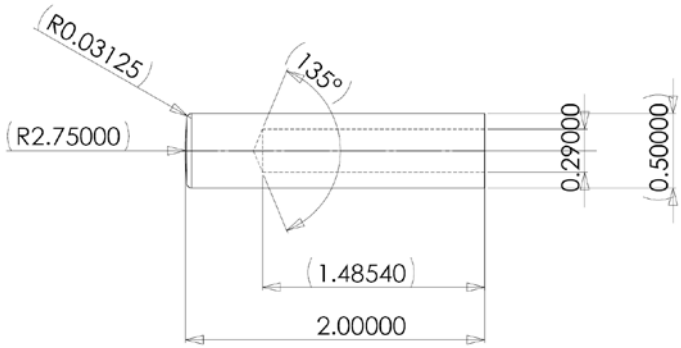

Figure A-3. Projectile 3 (37.5-g Straight/Hollow)

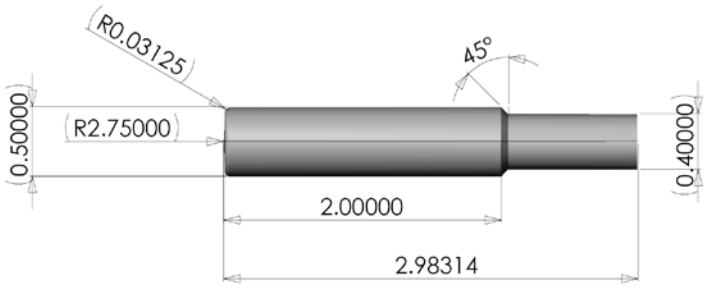

Figure A-4. Projectile 3a (37.5-g Straight/Extension)

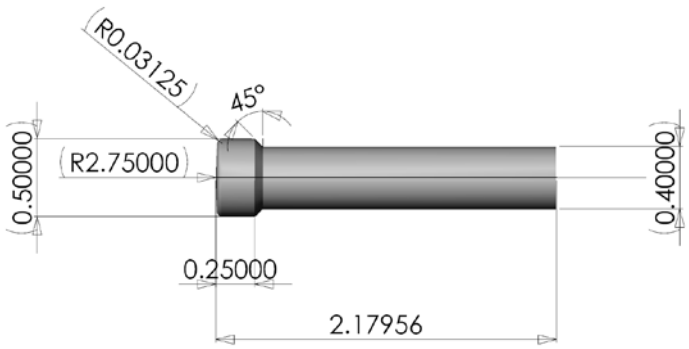

Figure A-5. Projectile 4 (37.5-g Stepped)

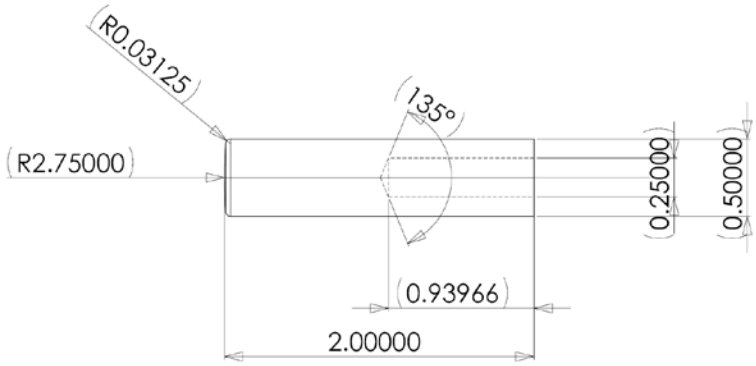

Figure A-6. Projectile 5 (25-g Straight/Hollow)

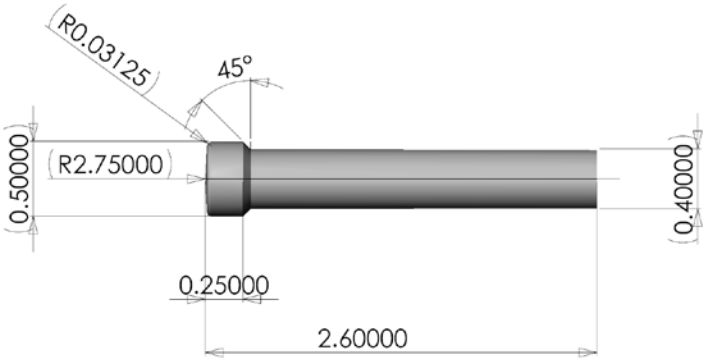

Figure A-7. Projectile 6 (25-g Stepped)

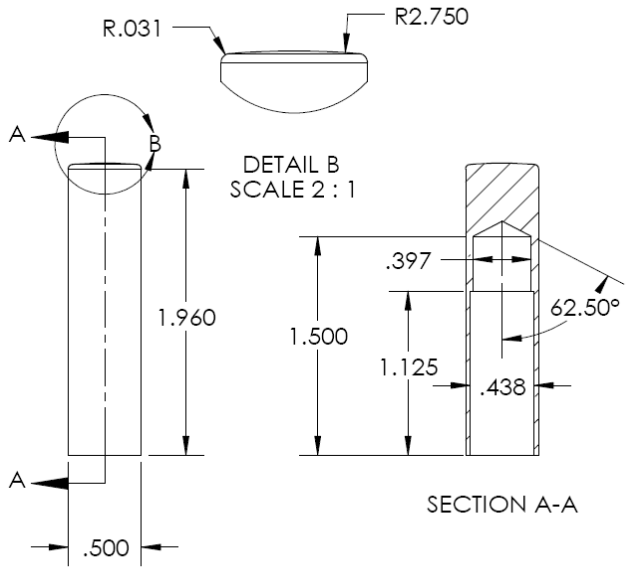

Figure A-8. Projectile 7a (12.5-g Straight/Hollow)

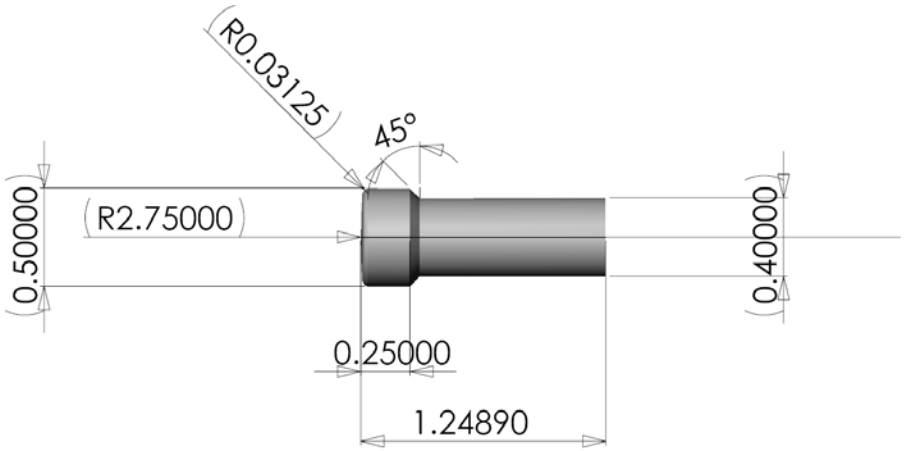

Figure A-9. Projectile 8 (12.5-g Stepped)

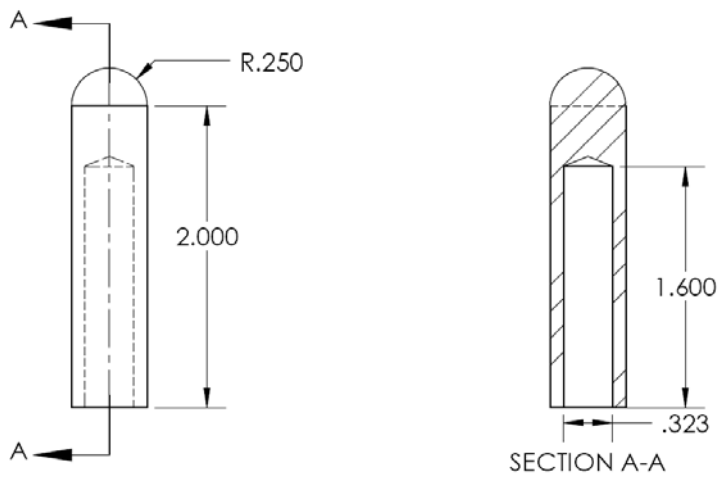

Figure A-10. Projectile 9 (37.5-g Straight/Hollow; Hemisphere)

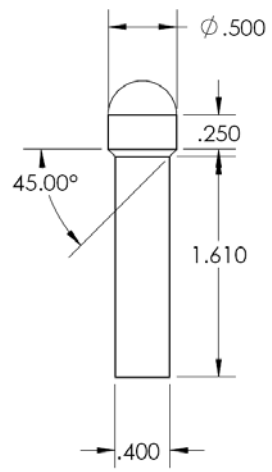

Figure A-11. Projectile 10 (37.5-g Stepped; Hemisphere)

APPENDIX B—PRESSURE, SPEED, AND ENERGY DATA

Table B-1. Pressure, Speed, and Energy Data for 50-g Projectiles With the National Aeronautics and Space Administration Flat End Used for Friction and Mass Study Impacting 6.35-mm-Thick 2024-T351 Aluminum

Projectile Description	Shot No.	Pressure (Mpa)	Projectile						Sabot	Plug		Absorbed Energy (including plug) (J)
			Initial Speed (m/s)	Initial Energy (J)	Final Speed (m/s)	Final Energy (J)	Energy Loss (J)	Penetration Angle (°)	Energy (J)	Speed (m/s)	Energy (J)	
Projectile 1: NASA Flat, straight, 50-g steel	1	2.98	133 ±4	444 ±24	-27 ±1	18 ±1	426 ±24			0	0	426 ±24
	5	3.27	146 ±3	528 ±20	50 ±2	62 ±4	466 ±20	9.4		58 ±2	4	462 ±20
	3	3.53	150 ±3	558 ±22	71 ±2	127 ±7	431 ±23	3.7		88 ±2	8	422 ±23
	4	3.50	150 ±3	558 ±22	76 ±2	145 ±8	413 ±24	4.9		88 ±2	9	404 ±24
	2	3.63	153 ±3	582 ±25	81 ±2	162 ±9	420 ±27	1.1		87 ±2	8	413 ±27
	9	4.02	160 ±3	636 ±24	92 ±3	210 ±12	426 ±27	4.4		99 ±3	11	415 ±27
	6	4.34	168 ±3	702 ±26	114 ±3	324 ±19	378 ±32	2.0		124 ±3	16	361 ±32
	7	5.05	178 ±3	789 ±29	123 ±4	374 ±22	415 ±36	3.4		140 ±4	20	394 ±36
	8	5.67	186 ±3	862 ±31	135 ±4	456 ±26	406 ±41	1.3		149 ±4	22	384 ±41
Projectile 2: NASA Flat, stepped, 50-g steel	4	3.29	140 ±3	491 ±19	-31 ±1	24 ±2	467 ±19		23	0	0	467 ±19
	1	3.50	146 ±3	528 ±21	60 ±2	90 ±5	438 ±22	6.9	25	83 ±2	7	431 ±22
	2	3.55	147 ±3	541 ±20	68 ±2	117 ±7	424 ±21	1.7	25	76 ±2	6	418 ±21
	3	3.61	147 ±3	541 ±20	64 ±2	103 ±6	439 ±21	3.0	25	80 ±2	7	432 ±21
	8	4.01	156 ±3	604 ±23	95 ±3	226 ±13	379 ±27	2.6	28	106 ±3	12	367 ±27
	5	4.32	159 ±3	634 ±23	106 ±3	279 ±16	355 ±28	0.5	30	118 ±3	14	340 ±28
	6	5.08	172 ±3	737 ±27	123 ±4	378 ±22	358 ±35	2.7	34	138 ±4	20	339 ±35
	7	5.70	182 ±4	826 ±32	138 ±4	477 ±28	349 ±43	0.7	39	165 ±4	27	321 ±43

Table B-2. Pressure, Speed, and Energy Data for 37.5-g Projectiles With NASA Flat End Used for Friction and Mass Study Impacting 6.35-mm-Thick 2024-T351 Aluminum

Projectile Description	Shot No.	Pressure (Mpa)	Projectile						Sabot	Plug		Absorbed Energy (including plug) (J)
			Initial Speed (m/s)	Initial Energy (J)	Final Speed (m/s)	Final Energy (J)	Energy Loss (J)	Penetration Angle (°)	Energy (J)	Speed (m/s)	Energy (J)	
Projectile 3: NASA Flat, straight/hollow, 37.5-g Steel	1	2.87	149 ±3	423 ±16	-36 ±1	25 ±2	398 ±16			0	0	398 ±16
	5	2.97	152 ±3	443 ±16	-29 ±1	16 ±1	426 ±16			0	0	426 ±16
	4	3.12	157 ±3	473 ±17	48 ±1	45 ±3	428 ±17	8.2		65 ±1	5	423 ±17
	3	3.28	161 ±3	494 ±18	55 ±2	58 ±3	436 ±18	4.1		93 ±2	10	426 ±18
	2	3.59	169 ±3	550 ±20	86 ±3	142 ±8	408 ±22	0.5		112 ±3	13	394 ±22
	6	4.32	181 ±3	630 ±23	121 ±3	281 ±16	349 ±28	1.4		138 ±3	20	329 ±28
	7	5.01	196 ±4	737 ±28	140 ±4	375 ±22	362 ±35	2.3		157 ±4	26	335 ±35
	8	5.73	210 ±4	849 ±31	159 ±5	486 ±28	363 ±42	0.7		172 ±5	31	332 ±42
	9	6.37	224 ±4	963 ±38	169 ±5	546 ±32	417 ±49	4.2		188 ±5	37	380 ±49
	1	7.02	230 ±4	1015 ±39	169 ±5	545 ±31	470 ±50	1.6		200 ±5	39	431 ±50
Projectile 3a: NASA Flat, straight/stepped, 37.5-g titanium	2	2.76	149 ±3	415 ±15	-39 ±2	28 ±2	386 ±15			0	0	386 ±15
	4	2.79	151 ±3	424 ±16	-25 ±1	12 ±1	413 ±16			0	0	413 ±16
	3	2.84	153 ±3	434 ±16	36 ±1	25 ±2	410 ±16	7.0		53 ±1	3	406 ±16
	1	2.92	156 ±3	453 ±17	47 ±1	41 ±3	411 ±18	5.8		75 ±1	6	405 ±18
	5	3.63	172 ±2	551 ±13	91 ±3	154 ±9	397 ±16	4.5		113 ±3	14	383 ±16
	6	4.29	178 ±2	591 ±13	102 ±3	195 ±11	396 ±18	4.1		117 ±3	15	381 ±18
	7	5.00	201 ±2	757 ±18	142 ±4	377 ±22	381 ±28	3.2		155 ±4	26	355 ±28
	8	5.74	216 ±2	871 ±20	158 ±5	464 ±27	406 ±33	1.6		175 ±5	32	374 ±33
	9	6.41	227 ±3	966 ±26	169 ±5	534 ±31	432 ±40	2.0		200 ±5	42	390 ±40
	10	7.18	237 ±3	1045 ±27	180 ±5	602 ±35	443 ±44	3.1		214 ±5	46	397 ±44
Projectile 4: NASA Flat, stepped, 37.5-g titanium	8	2.78	146 ±3	399 ±15	-40 ±1	30 ±2	368 ±15		25	0	0	368 ±15
	7	2.97	151 ±3	428 ±16	8 ±1	1 ±0	426 ±16	4.0	26	9 ±1	0	426 ±16
	6	3.63	165 ±3	510 ±18	100 ±3	188 ±11	322 ±21	1.9	32	109 ±3	13	309 ±21
	5	4.41	182 ±3	623 ±23	127 ±4	305 ±18	317 ±29	4.3	39	136 ±4	19	299 ±29
	4	4.98	194 ±4	709 ±27	142 ±4	379 ±22	330 ±35	1.9	44	159 ±4	25	305 ±35
	3	5.69	206 ±4	800 ±30	163 ±5	502 ±29	298 ±42	3.7	50	163 ±5	29	269 ±42
	2	6.37	221 ±4	917 ±33	173 ±5	564 ±33	353 ±46	3.3	57	185 ±5	36	318 ±46
	1	7.14	227 ±4	973 ±38	180 ±5	612 ±35	361 ±52	2.9	60	191 ±5	38	324 ±52

Table B-3. Pressure, Speed, and Energy Data for 25-g Projectiles With NASA Flat End Used for Friction and Mass Study Impacting 6.35-mm-Thick 2024-T351 Aluminum

Projectile Description	Shot No.	Pressure (Mpa)	Projectile					Sabot	Plug		Absorbed Energy (including plug) (J)
			Initial Speed (m/s)	Initial Energy (J)	Final Speed (m/s)	Final Energy (J)	Energy Loss (J)	Energy (J)	Speed (m/s)	Energy (J)	
Projectile 5: NASA Flat, straight/hollow, 25-g titanium	4	2.37	169 ±3	355 ±13	-29 ±1	10 ±1	345 ±13		0	0	345 ±13
	9	2.50	169 ±3	354 ±12	-32 ±1	13 ±1	341 ±12		0	0	341 ±12
	3	2.52	178 ±3	391 ±13	36 ±1	16 ±1	374 ±13		67 ±1	5	369 ±13
	2	2.74	183 ±3	416 ±15	67 ±2	56 ±3	360 ±15		98 ±2	10	350 ±15
	1	2.87	183 ±2	416 ±9	74 ±1	67 ±2	349 ± 9		99 ±1	11	338 ±9
	5	3.55	201 ±2	502 ±10	120 ±1	177 ±3	325 ±10		143 ±1	22	303 ±10
	6	4.30	225 ±2	626 ±14	151 ±1	283 ±4	342 ±14		172 ±1	29	313 ±14
	7	5.03	239 ±2	708 ±14	153 ±2	290 ±6	418 ±16		196 ±2	39	379 ±16
	8	5.77	257 ±3	818 ±19	175 ±2	378 ±7	441 ±21		228 ±2	52	389 ±21
	10	6.43	266 ±3	876 ±20	187 ±2	435 ±7	442 ±21		239 ±2	57	385 ±21
Projectile 6: NASA Flat, stepped, 25-g titanium	2	2.44	165 ±3	338 ±12	-28 ±1	10 ±1	329 ±12	32	0	0	329 ±12
	3	2.61	170 ±3	360 ±13	-29 ±1	11 ±1	349 ±13	34	0	0	349 ±13
	1	2.73	175 ±3	382 ±13	42 ±1	22 ±1	360 ±13	36	56 ±1	3	357 ±13
	4	2.99	184 ±3	423 ±15	85 ±2	90 ±5	332 ±16	39	96 ±2	10	323 ±16
	5	3.62	201 ±4	506 ±19	119 ±3	176 ±10	330 ±22	47	147 ±3	23	306 ±22
	6	4.41	218 ±4	595 ±22	149 ±4	276 ±16	319 ±27	56	151 ±4	24	294 ±27
	7	5.03	230 ±4	663 ±24	164 ±5	336 ±20	327 ±31	62	194 ±5	39	287 ±31
	8	5.72	250 ±4	779 ±27	180 ±5	402 ±24	377 ±36	73	216 ±5	48	329 ±36

Table B-4. Pressure, Speed, and Energy Data for 12.5-g Projectiles With NASA Flat End Used for Friction and Mass Study Impacting 6.35-mm-Thick 2024-T351 Aluminum

Projectile Description	Shot No.	Pressure (Mpa)	Projectile					Sabot	Plug		Absorbed Energy (including plug) (J)
			Initial Speed (m/s)	Initial Energy (J)	Final Speed (m/s)	Final Energy (J)	Energy Loss (J)	Energy (J)	Speed (m/s)	Energy (J)	
Projectile 7: NASA Flat, straight/hollow, 12.5-g titanium	5	1.92	218 ±4	287 ±11	-24 ±1	4 ±0	283 ±11		0	0	283 ±11
	2	2.28	240 ±4	350 ±12	-25 ±1	4 ±0	347 ±12		0	0	347 ±12
	6	2.41	238 ±4	342 ±13	-26 ±1	4 ±0	338 ±13		0	0	338 ±13
	4	2.62	252 ±5	385 ±16	91 ±3	50 ±3	334 ±16		121 ±3	15	320 ±16
	8	2.69	258 ±5	402 ±15	97 ±3	57 ±3	345 ±15		127 ±3	16	329 ±15
	9	3.10	269 ±5	438 ±16	123 ±4	92 ±5	346 ±16		150 ±4	23	324 ±16
	3	2.99	271 ±5	445 ±18	0 ±0	0 ±0	445 ±18		127 ±0	16	429 ±18
	10	3.45	279 ±6	469 ±19	137 ±4	113 ±7	357 ±20		157 ±4	25	332 ±20
	1	3.66	294 ±6	523 ±20	63 ±2	24 ±1	500 ±20		136 ±2	18	481 ±20
	7	4.32	313 ±6	594 ±22	182 ±5	201 ±12	393 ±25		215 ±5	46	346 ±25
Projectile 8: NASA Flat, stepped, 12.5-g titanium	1	1.62	180 ±3	205 ±7	-26 ±1	4 ±0	201 ± 7	38	0	0	201 ±7
	2	2.24	180 ±3	204 ±7	-24 ±3	4 ±1	201 ± 7	38	0	0	201 ±7
	5	2.43	220 ±4	307 ±10	-29 ±1	5 ±0	301 ±10	57	0	0	301 ±10
	4	2.63	230 ±4	335 ±12	56 ±2	20 ±1	316 ±12	62	64 ±2	4	311 ±12
	3	2.96	238 ±4	357 ±13	109 ±3	75 ±4	282 ±13	66	129 ±3	18	264 ±13
	6	3.61	267 ±6	450 ±19	154 ±4	149 ±9	301 ±21	83	160 ±4	27	274 ±21
	7	4.30	291 ±6	535 ±21	175 ±5	193 ±11	342 ±24	99	183 ±5	34	308 ±24
	8	4.99	315 ±6	628 ±24	183 ±5	212 ±12	416 ±27	116	218 ±5	47	369 ±27

Table B-5. Pressure, Speed, and Energy Data for 37.5-g Projectiles With Hemispherical End Used for Friction and Mass Study Impacting 6.35-mm-Thick 2024-T351 Aluminum

Projectile Description	Shot No.	Pressure (Mpa)	Projectile					Sabot	Plug		Absorbed Energy (including plug) (J)
			Initial Speed (m/s)	Initial Energy (J)	Final Speed (m/s)	Final Energy (J)	Energy Loss (J)	Energy (J)	Speed (m/s)	Energy (J)	
Projectile 9: Hemispherically tipped, straight/hollow, 37.5-g steel	1	2.83	149 ± 3	414 ± 14	-30 ± 1	17 ± 1	397 ± 15		0	0	397 ± 15
	2	2.95	154 ± 3	438 ± 16	-30 ± 1	17 ± 1	421 ± 16		0	0	421 ± 16
	3	3.32	162 ± 3	488 ± 17	-32 ± 1	19 ± 1	469 ± 17		0	0	469 ± 17
	4	3.56	169 ± 3	530 ± 19	-33 ± 1	20 ± 1	510 ± 19		0	0	510 ± 19
	5	3.90	177 ± 3	583 ± 21	-27 ± 1	13 ± 1	570 ± 21		103 ± 1	11	558 ± 21
	6	4.22	181 ± 3	610 ± 22	0 ± 0	0 ± 0	610 ± 22		94 ± 0	9	601 ± 22
	7	5.02	199 ± 3	736 ± 26	0 ± 0	0 ± 0	736 ± 26		127 ± 0	16	720 ± 26
	8	5.63	211 ± 4	827 ± 28	73 ± 2	99 ± 6	729 ± 29		149 ± 2	22	706 ± 29
	9	6.37	220 ± 4	897 ± 32	103 ± 3	196 ± 12	701 ± 34		164 ± 3	27	674 ± 34
	10	7.05	233 ± 4	1008 ± 39	128 ± 4	303 ± 18	704 ± 43		184 ± 4	34	671 ± 43
Projectile 10: Hemispherically tipped, stepped, 37.5-g steel	1	2.97	149 ± 3	411 ± 14	-28 ± 1	14 ± 1	397 ± 14	26	0	0	397 ± 14
	2	3.68	168 ± 3	526 ± 19	-32 ± 1	19 ± 1	506 ± 19	33	0	0	506 ± 19
	3	4.00	177 ± 3	581 ± 20	-30 ± 1	16 ± 1	565 ± 20	36	88 ± 1	8	557 ± 20
	4	4.34	175 ± 3	570 ± 20	-29 ± 1	15 ± 1	555 ± 20	36	51 ± 1	3	552 ± 20
	5	5.03	196 ± 3	715 ± 25	69 ± 2	90 ± 5	626 ± 26	45	131 ± 2	17	609 ± 26
	6	5.66	206 ± 4	791 ± 27	93 ± 3	162 ± 10	629 ± 29	50	137 ± 3	19	610 ± 29
	7	6.39	228 ± 4	967 ± 34	124 ± 4	285 ± 17	683 ± 38	61	157 ± 4	25	658 ± 38
	8	7.07	230 ± 4	988 ± 35	139 ± 4	360 ± 21	628 ± 41	62	171 ± 4	29	599 ± 41

Table B-6. Pressure, Speed, and Energy Data for 9.9-g NASA Flat Projectiles Penetrating 3.18-mm NASA 2024-T3 Aluminum Sheet

Projectile Description	Shot No.	Pressure (Mpa)	Projectile						Plug			Absorbed Energy (including plug) (J)
			Mass (g)	Initial Speed (m/s)	Initial Energy (J)	Final Speed (m/s)	Final Energy (J)	Energy Loss (J)	Mass (g)	Speed (m/s)	Energy (J)	
NASA Flat, 3.18-mm sheet, 9.9-g projectile	5	1.38	9.9	180	161	0	0	161	0.0	0	0	161
	6	1.55	9.9	196	190	0	0	190	0.0	0	0	190
	13	1.55	9.9	200	198	0	0	198	0.0	0	0	198
	4	*1.72*	*9.9*	*206*	*210*	*73*	*26*	*184*	*2.0*	*35*	*1*	*183*
	7	1.72	9.9	209	216	0	0	216	0.0	0	0	216
	25	1.72	9.9	212	222	0	0	222	0.0	0	0	222
	12	1.79	9.9	218	236	98	48	189	1.0	122	7	181
	11	*1.90*	*9.9*	*222*	*243*	*55*	*15*	*228*	*2.0*	*15*	*0.2*	*228*
	8	2.07	9.9	225	250	108	58	191	1.0	160	13	179
	28	*2.07*	*9.9*	*230*	*261*	*113*	*64*	*198*	*2.0*	*113*	*13*	*185*
	27	2.48	9.9	252	313	174	150	163	1.0	190	18	145
	26	2.48	9.9	254	319	173	148	171	1.0	204	21	150
	2	2.76	9.9	259	333	193	185	148	1.0	238	28	120
	1	3.45	9.9	314	490	244	295	195	1.0	264	35	160
	9	4.83	9.9	355	623	303	454	169	1.0	325	53	116
	10	6.21	9.9	381	718	342	578	140	1.0	364	66	74

Note: Data given in italics are for projectiles that impacted the target at a sufficient angle to cause a larger than normal plug with a figure-eight shape. All other plugs had a circular cross section.

Table B-7. Pressure, Speed, and Energy Data for 9.85-g Hemispherically Tipped Projectiles Penetrating 3.18-mm NASA 2024-T3 Aluminum Sheet

Projectile Description	Shot No.	Pressure (Mpa)	Projectile						Plug			Absorbed Energy (including plug) (J)
			Mass (g)	Initial Speed (m/s)	Initial Energy (J)	Final Speed (m/s)	Final Energy (J)	Energy Loss (J)	Mass (g)	Speed (m/s)	Energy (J)	
Hemispherically tipped, 3.18-mm sheet, 9.85-g projectile	4	2.07	9.85	147	107	0	0	107	1.0	0	0	107
	6	2.41	9.85	196	190	0	0	190	1.0	165	14	176
	3	2.76	9.85	202	202	12	1	201	1.0	174	15	186
	12	2.83	9.85	209	215	51	13	202	1.0	176	15	186
	11	2.90	9.85	219	236	97	46	189	1.0	186	17	172
	13	2.69	9.85	228	256	119	70	186	1.0	197	19	167
	9	3.45	9.85	232	265	126	78	187	1.0	201	20	166
	10	3.10	9.85	240	283	144	102	180	1.0	210	22	158
	2	4.14	9.85	274	370	186	171	199	1.0	253	32	167
	7	4.83	9.85	309	471	211	219	251	1.0	267	36	216
	8	5.52	9.85	326	524	232	265	258	1.0	286	41	218
	14	6.90	9.85	342	577	280	386	191	1.0	319	51	140
	1	6.28	9.85	347	592	273	368	224	1.0	311	48	176

Table B-8. Pressure, Speed, and Energy Data for 13-g NASA Flat Projectiles Penetrating 6.35-mm NASA 2024-T351 Aluminum Plate

Projectile Description	Shot No.	Pressure (Mpa)	Projectile						Plug			Absorbed Energy (including plug) (J)
			Mass (g)	Initial Speed (m/s)	Initial Energy (J)	Final Speed (m/s)	Final Energy (J)	Energy Loss (J)	Mass (g)	Speed (m/s)	Energy (J)	
NASA Flat, 6.35-mm plate, 13-g projectile	8	2.34	13	231	346	0	0	346	2.0	72	5	341
	7	2.34	13	231	346	45	13	333	2.0	72	5	328
	6	2.34	13	231	346	0	0	346	2.0	0	0	346
	10	2.59	13	243	384	82	43	340	2.0	112	13	328
	12	2.59	13	243	384	57	21	363	2.0	84	7	356
	11	2.59	13	243	384	28	5	378	2.0	98	10	369
	23		13	272	480	127	105	375	2.0	177	31	343
	31	5.17	13	317	654	204	269	385	2.0	242	58	326
	32	5.69	13	326	693	215	301	392	2.0	248	62	331
	33	6.28	13	346	778	230	343	435	2.0	265	70	365
	35	6.90	13	360	843	242	382	462	2.0	270	73	389
	22		13	361	846	246	392	454	2.0	292	85	368
	34	7.69	13	377	923	260	439	484	2.0	297	88	396
	20		13	417	1133	288	541	592	2.0	326	107	486
	21		13	429	1199	303	597	602	2.0	326	107	495

Table B-9. Pressure, Speed, and Energy Data for 13-g Hemispherically Tipped Projectiles Penetrating 6.35-mm NASA 2024-T351 Aluminum Plate

Projectile Description	Shot No.	Pressure (Mpa)	Projectile						Plug			Absorbed Energy (including plug) (J)
			Mass (g)	Initial Speed (m/s)	Initial Energy (J)	Final Speed (m/s)	Final Energy (J)	Energy Loss (J)	Mass (g)	Speed (m/s)	Energy (J)	
Hemispherically tipped, 6.35-mm plate, 13-g projectile	13	2.59	13	234	356	0	0	356	1.4	0	0	356
	14	2.59	13	235	359	0	0	359	1.4	0	0	359
	15	2.59	13	246	394	0	0	394	1.4	0	0	394
	15	3.62	13	274	487	0	0	487	1.4	98	7	480
	17	5.00	13	320	667	0	0	667	1.4	219	34	634
	18	8.10	13	394	1011	221	319	693	1.4	295	61	632
	39	9.00	13	402	1049	241	376	673	1.4	335	78	594
	38	9.66	13	414	1117	263	449	668	1.4	313	68	599
	37	10.34	13	424	1167	278	503	665	1.4	336	79	586
	36	11.03	13	436	1234	298	579	655	1.4	355	88	567

Table B-10. Pressure, Speed, and Energy Data for 28-g NASA Flat Projectiles Penetrating 12.7-mm NASA 2024-T351 Aluminum Plate

Projectile Description	Shot No.	Pressure (Mpa)	Projectile						Plug			Absorbed Energy (including plug) (J)
			Mass (g)	Initial Speed (m/s)	Initial Energy (J)	Final Speed (m/s)	Final Energy (J)	Energy Loss (J)	Mass (g)	Speed (m/s)	Energy (J)	
NASA Flat, 12.7-mm plate, 28-g projectile	2	6.55	28	245	838	0	0	838	4.0	0	0	838
	6	6.90	28	248	860	0	0	860	4.0	57	6	853
	3	7.24	28	259	942	0	0	942	4.0	0	0	942
	8	7.76	28	262	959	0	0	959	4.0	111	25	935
	4	7.59	28	262	961	0	0	961	4.0	77	12	950
	7	7.41	28	263	967	0	0	967	4.0	114	26	941
	1	7.93	28	265	984	51	36	948	4.0	143	41	907
	9	8.28	28	274	1053	0	0	1053	4.0	143	41	1012
	5	8.62	28	278	1080	90	114	966	4.0	147	43	923

APPENDIX C—STATISTICAL ANALYSIS USING THE R SOFTWARE PACKAGE

C.1 COMPARISON OF STEEL AND TITANIUM PROJECTILES (STRAIGHT; 37.5 g).

Table C-1 shows the penetration data for projectiles 3 and 3a. This file is used to compare the effect of material in otherwise identical projectiles.

Table C-1. Material_37g.csv Data File

Mass (g)	Initial Energy (J)	Energy Absorbed (J)	Shape	Material
37.5	434	406	Straight	Titanium
37.5	453	405	Straight	Titanium
37.5	1045	397	Straight	Titanium
37.5	966	390	Straight	Titanium
37.5	551	383	Straight	Titanium
37.5	591	381	Straight	Titanium
37.5	871	374	Straight	Titanium
37.5	757	355	Straight	Titanium
37.5	1015	431	Straight	Steel
37.5	494	426	Straight	Steel
37.5	473	423	Straight	Steel
37.5	550	394	Straight	Steel
37.5	963	380	Straight	Steel
37.5	737	335	Straight	Steel
37.5	849	332	Straight	Steel
37.5	630	329	Straight	Steel

The following presents the R code and results used to examine the effect of material on absorbed energy.

- Two-sample t-test

```
> energy_data = read.csv( "Material_37g.csv", header = TRUE)

> tapply(energy_data$Energy, energy_data$Material, mean)
         Steel Titanium
       381.250  386.375

> tapply(energy_data$Energy, energy_data$Material, sd)
         Steel Titanium
      44.20650 17.05401

> t.test(energy_data$Energy ~ energy_data$Material, var.equal = TRUE)

              Two Sample t-test

      data:  energy_data$Energy by energy_data$Material
      t = -0.3059, df = 14, p-value = 0.7642
      alternative hypothesis:  true difference in means is not equal to 0
      95 percent confidence interval:
       -41.05461  30.80461
      sample estimates:
         mean in group Steel mean in group Titanium
                     381.250                386.375
```

- Linear regression

```
> fit_mat = lm(Energy ~ Initial + I(Initial^2) + Material, data = energy_data)

> summary(fit_mat)

      Call:
      lm(formula = Energy ~ Initial + I(Initial^2) + Material, data = energy_data)

      Residuals:
          Min      1Q  Median      3Q     Max
      -30.985 -14.819   5.935  13.452  25.221

      Coefficients:
         Estimate   Std.  Error   t value   Pr(>|t|)
      (Intercept)       8.113e+02    8.437e+01     9.616   5.46e-07 ***
      Initial          -1.235e+00    2.430e-01    -5.081   0.000270 ***
      I(Initial^2)      8.230e-04    1.647e-04     4.996   0.000311 ***
      MaterialTitanium -3.013e+00    1.027e+01    -0.293   0.774274
      ---
      Signif.  codes:  0 ‘***’ 0.001 ‘**’ 0.01 ‘*’ 0.05 ‘.’ 0.1 ‘ ’ 1

      Residual standard error:  20.29 on 12 degrees of freedom
      Multiple R-squared:  0.6877,     Adjusted R-squared:  0.6097
      F-statistic:  8.809 on 3 and 12 DF,  p-value:  0.002326
```

C.2 ANALYSIS TO DETERMINE EFFECT OF PROJECTILE SHAPE AND MASS.

Table C-2. Mass_Energy_Shape_Material.csv Data File for Mass and Shape Analysis

Mass (g)	Initial Energy (J)	Energy Absorbed (J)	Shape	Material
50	528	462	Straight	Steel
50	558	422	Straight	Steel
50	558	404	Straight	Steel
50	582	413	Straight	Steel
50	636	415	Straight	Steel
50	702	361	Straight	Steel
50	789	394	Straight	Steel
50	862	384	Straight	Steel
50	528	431	Stepped	Steel
50	541	432	Stepped	Steel
50	541	418	Stepped	Steel
50	604	367	Stepped	Steel
50	634	340	Stepped	Steel
50	737	339	Stepped	Steel
50	826	321	Stepped	Steel
37.5	473	423	Straight	Steel
37.5	494	426	Straight	Steel
25	663	287	Stepped	Titanium
25	779	329	Stepped	Titanium
12.5	385	320	Straight	Titanium
12.5	402	329	Straight	Titanium
12.5	438	324	Straight	Titanium
12.5	445	429	Straight	Titanium
12.5	469	332	Straight	Titanium
12.5	523	481	Straight	Titanium
12.5	594	346	Straight	Titanium
12.5	335	311	Stepped	Titanium
12.5	357	264	Stepped	Titanium
12.5	450	274	Stepped	Titanium
12.5	535	308	Stepped	Titanium
12.5	628	369	Stepped	Titanium

Note: Not all rows are shown for the 37.5- and 25-g projectiles. The complete data set is available in appendix B.

The following presents the R code and results used to examine the effect of shape (and mass) on absorbed energy.

- Two-sample t-test

```
> energy_data = read.csv( "Mass_Energy_Shape_Material.csv", header = TRUE)

> tapply(energy_data$Energy, energy_data$Shape, mean)
       Stepped Straight
      332.8000 379.0513

> tapply(energy_data$Energy, energy_data$Shape, sd)
       Stepped Straight
      49.70161 41.88892

> t.test(energy_data$Energy ~ energy_data$Material, var.equal = TRUE)

              Two Sample t-test

      data:  energy_data$Energy by energy_data$Material
      t = 3.7023, df = 62, p-value = 0.0004565
      alternative hypothesis:  true difference in means is not equal to 0
      95 percent confidence interval:
       20.30691 67.97092
      sample estimates:
         mean in group Steel mean in group Titanium
                    389.2609               345.1220
```

- Linear regression

```
> fit_shape = lm(Energy ~ Initial + Shape + Mass + I(Initial^2), data = energy_data)

> summary(fit_shape)

      Call:
      lm(formula  =  Energy  ~  Initial  +  Shape  +  Mass  +  I(Initial^2),  data  =
      energy_data)

      Residuals:
          Min      1Q  Median      3Q     Max
      -65.578 -28.292  -6.647  15.582 139.326

      Coefficients:
                      Estimate Std.  Error t value Pr(>|t|)
      (Intercept)    3.774e+02  6.689e+01   5.643 5.01e-07 ***
      Initial       -3.017e-01  2.195e-01  -1.375    0.174
      ShapeStraight  4.693e+01  1.032e+01   4.546 2.77e-05 ***
      Mass           1.964e+00  4.465e-01   4.397 4.64e-05 ***
      I(Initial^2)   1.848e-04  1.585e-04   1.166    0.248
      ---
      Signif.  codes:  0 ‘***’ 0.001 ‘**’ 0.01 ‘*’ 0.05 ‘.’ 0.1 ‘ ’ 1

      Residual standard error:  40.06 on 59 degrees of freedom
      Multiple R-squared:  0.4027,     Adjusted R-squared:  0.3622
      F-statistic:  9.945 on 4 and 59 DF,  p-value:  3.216e-06
```

C.3 ANALYSIS TO DETERMINE EFFECT OF SHAPE USING HEMISPHERICAL TIPPED PROJECTILES.

Table C-3. Hemi_37g.csv Data File for Comparing Energy Loss in Penetration of Hemispherical, Stepped vs. Straight Projectiles

Initial Energy (J)	Energy Absorbed (J)	Shape
827	706	Straight
897	674	Straight
1008	671	Straight
715	609	Stepped
791	610	Stepped
967	658	Stepped
988	599	Stepped

The following presents the R code and results used to examine the effect of shape on absorbed energy.

- Two-sample t-test

```
> hemi_data = read.csv( "Hemi_37g.csv", header = TRUE)

> tapply(hemi_data$Energy, hemi_data$Shape, mean)
        Stepped Straight
       619.0000 683.6667

> tapply(hemi_data$Energy, hemi_data$Shape, sd)
        Stepped Straight
       26.47011 19.39931

> t.test(hemi_data$Energy ~ hemi_data$Shape, var.equal = TRUE)

                Two Sample t-test

       data:  hemi_data$Energy by hemi_data$Shape
       t = -3.5435, df = 5, p-value = 0.0165
       alternative hypothesis:  true difference in means is not equal to 0
       95 percent confidence interval:
        -111.57851  -17.75482
       sample estimates:
        mean in group Stepped mean in group Straight
                     619.0000               683.6667
```